

# Radar-enabled ambient backscatter communication

Luca Venturino, *Senior Member, IEEE*, Emanuele Grossi, *Senior Member, IEEE*,  
Marco Lops, *Fellow, IEEE*, Jeremy Johnston, Xiaodong Wang, *Fellow, IEEE*

## Abstract

In this work, we exploit the radar clutter (i.e., the ensemble of echoes generated by the terrain and/or the surrounding objects in response to the signal emitted by a radar transmitter) as a carrier signal to enable an ambient backscatter communication from a source (tag) to a destination (reader). Upon deriving a convenient signal model, we exploit the fact that the radar clutter is periodic over time scales shorter than the coherence time of the environment, because so is the radar excitation, to distinguish the message sent by the tag from the superimposed ambient interference. In particular, we propose two encoding/decoding schemes that do not require any coordination with the radar transmitter or knowledge of the radar waveform. Different tradeoffs in terms of transmission rate and error probability can be obtained upon changing the control signal driving the tag switch or the adopted encoding rule; also, multiple tags can be accommodated with either a sourced or an unsourced multiple access strategy.

## Index Terms

Ambient backscatter, tag, radar and communication spectrum sharing, clutter, sourced/unsourced multiple access.

## I. INTRODUCTION

Communications and radar have historically followed parallel paths, which intersected only occasionally, until the emerging Internet of Things (IoT) and perceptive mobile networks

L. Venturino and E. Grossi are with the Department of Electrical and Information Engineering, University of Cassino and Southern Lazio, 03043 Cassino, Italy, and with CNIT, 43124 Parma, Italy (e-mail: l.venturino@unicas.it; e.grossi@unicas.it). J. Johnston and X. Wang are with the Department of Electrical Engineering, Columbia University, New York, NY 10027, United States (e-mail: j.johnston@columbia.edu; xw2008@columbia.edu). M. Lops is with the Department of Electrical and Information Technology, University of Naples Federico II, 80138 Naples, Italy, and with CNIT, 43124 Parma, Italy (e-mail: lops@unina.it).

have tightly intertwined them [1]–[3] to support a number of advanced applications (such as, e.g., autonomous driving, smart cities/factories, environmental/home monitoring, healthcare). Spectrum overcrowding has been the inevitable counterbalance to these developments, posing new challenges for a more efficient exploitation of the available spectrum *and* a containment of operational costs, power consumption, and electromagnetic emissions.

A response to these challenges has been the paradigm shift from spectrum sharing between two autonomous systems, possibly exchanging information and interacting with each other [4], to integrated sensing and communication (ISAC) architectures [5], [6] encompassing just one active transmitter and two different receiving chains to accommodate the two functions. The transmitter may be designed *ad hoc* by resorting to suitable waveforms and beamforming strategies, and the resources allocated to the two functions are determined based on the required quality of service.

A far less costly strategy relies on the exploitation of signals of opportunity—typically, the signal emitted by TV/FM towers, cellular base stations, and Wi-Fi access points—to implement a passive radar, which has the merit of being low-cost, difficult to jam, easy to deploy, and undetectable [7]. To the family of passive radars can be somehow ascribed the *opportunistic* architectures considered in [8]–[11], mainly with reference to automotive applications through millimeter-wave (mmWave) communication signals: in close proximity with the communication transmitter, a radar receive chain, which may avail itself of information shared by the transmitter, implements the sensing function without producing interference and without requiring any additional physical resource. In particular, [12] puts forward mmWave communication signals as the only credible means to support massive automotive sensing.

The reverse paradigm of radar-enabled communications has been less explored. Even though the idea has been proposed back in the 1940's [13], only in the past two decades have systematic studies on the matter emerged. For example, it has been suggested in [14] that targets in synthetic aperture radar (SAR) images can be tagged for unambiguous identification and localization by equipping them with a radio-frequency (RF) transponder that downconverts, encodes, and retransmits the received probing signal; in particular, the proposed scheme assigns to each target a unique Golay code, which modulates consecutive radar pulses. Also, [15]–[17] have investigated covert communications embedded in radar reverberation (clutter). Here a RF transponder, relying on knowledge of the radar signal and making suitable assumptions on the clutter process, undertakes an *ad hoc* remodulation and retransmission of a single radar pulse; the transponder consists of a complete RF receive/transmit chain and operates on a wider bandwidth than that

of the radar to create the necessary degrees of freedom.

The idea of exploiting astray signals also underlies the so-called ambient backscatter communications, that rely on low-cost and low-power modulators, often not connected to a battery or a power grid. For example, [18]–[20] show that signals broadcast from existing communication sources can be successfully exploited for short range data transmission in many IoT applications. Instead, [21] considers a radar base station employing a frequency-modulated continuous-wave signal for joint ranging and data transfer from the backscatter modulator of multiple sensor nodes; here, the tag modulates the direct radar signal (not the echoes from the surrounding objects), while the reader knows the radar waveform and its timing.

The focus of this paper is on ambient backscatter communication using radar reverberation as a carrier signal. A radar always transmits a periodic signal, which may be for example a low duty cycle pulse train or a modulated continuous wave. Any object located inside a scene illuminated by a radar transmitter inevitably produces scattering in all directions [22], [23]: for example, densely populated areas generate an overwhelming land clutter, i.e., reflections from static (or almost static, if the wind effect is taken into account) objects, such as walls, buildings, vegetation, man-made infrastructures, mountains, and so on. An ambient backscatterer (hereafter referred to as a tag) immersed in clutter on a continuous or almost so basis is endowed with a “natural” carrier signal that can be modulated for conveying information towards a receiver (hereafter referred to as a reader). Similarly, the reverberation generated by a radar transmitter hits the reader, whereby a signal-dependent interference is superimposed on the signal of interest arriving from the tag. Hence, the radar clutter is here both a friend (as it provides an ambient carrier signal at the transmit side) and a foe (as it causes interference at the receiver side). The key point is that the clutter—when observed on conveniently short time intervals—reproduces the *periodic structure* of the original radar signal. In what follows, we formulate the problem of designing and assessing radar-enabled backscatter communications under two key constraints:

- The backscatter modulator of the tag does not use any RF processing chain, but can only vary the phase/amplitude of the impinging signal at a pre-determined rate.
- The tag and the reader know the radar period and the channel coherence time; however, they have no information as to the actual radar waveform and the impinging clutter (i.e., no channel state information is available for the radar-tag-reader and the radar-reader links), so that coordination with the radar transmitter is not required.

Under this scenario, the contributions of the present study can be summarized as follows:

- We elaborate a convenient signal model and illustrate the interplay among the key system parameters, such as the bandwidth and the period of the radar waveform, the symbol rate employed by the modulator, the duty-cycle of the control signal driving the tag switch, the bandwidth and duration of the receive filter, and the sampling rate. In particular, we show that the unknown baseband pulses carrying the data symbols in the backscattered signal present a periodic structure induced by the radar excitation.
- We propose encoding/decoding strategies which use a discrete set of reflection coefficients at the tag and are resilient against the radar interference hitting the reader. In particular, we present a promising scheme coupling binary orthogonal coding through the columns of a Hadamard matrix with a differential phase shift keying (PSK) modulation.
- We show that the proposed setup carries over plainly to the situation where simultaneous transmissions from multiple synchronous tags must be guaranteed with either a sourced or an unsourced multiple access strategy.
- Finally, we provide some illustrative examples to assess the effectiveness of the proposed signaling schemes and show some achievable tradeoffs among transmission rate, error probability, and number of supported tags.

The remainder of the paper is organized as follows. Sec. II contains the system description and the signal model development. Sec. III presents the encoding/decoding schemes. Sec. IV considers the presence of multiple tags. Sec. V contains the performance analysis. Finally, Sec. VI gives some concluding remarks, while the Appendix contains some analytical proofs.

*Notation:* In the following,  $\mathbb{N}$ ,  $\mathbb{Z}$ , and  $\mathbb{C}$  are the set of natural, integer, and complex numbers, respectively. Column vectors and matrices are denoted by lowercase and uppercase boldface letters, respectively. The symbols  $\Re\{\cdot\}$ ,  $(\cdot)^*$ ,  $(\cdot)^T$ , and  $(\cdot)^H$  denotes real part, conjugate, transpose, and conjugate-transpose, respectively.  $\mathbf{1}_M$  and  $\mathbf{0}_M$ , are the  $M$ -dimensional all-one and all-zero column vectors, respectively.  $a_i$  are  $\|\mathbf{a}\|$  are the  $i$ -th entry and the Euclidean norm of the vector  $\mathbf{a}$ .  $\|\mathbf{A}\|_F$ ,  $\text{Rank}\{\mathbf{A}\}$ ,  $\text{Tr}\{\mathbf{A}\}$ , and  $\mathbf{A}^\dagger$  are the Frobenius norm, the rank, the trace, and the pseudoinverse of the matrix  $\mathbf{A}$ .  $\mathbf{I}_M$  is the  $M \times M$  identity matrix.  $\chi_k^2$  denotes the chi-squared distribution with  $k$  degrees of freedom.  $\chi_k^2(\lambda)$  denotes the noncentral chi-squared distribution with  $k$  degrees of freedom and noncentrality parameter  $\lambda$ .  $I_k(\cdot)$  is the modified Bessel function of the first kind and order  $k$ . Finally,  $i$ ,  $\star$ , and  $\text{E}[\cdot]$  denotes the imaginary unit, the convolution operator, and the statistical expectation, respectively.

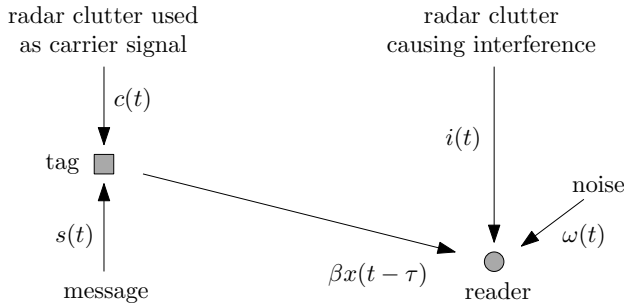


Figure 1. Graphical illustration of the proposed radar-enabled ambient backscatter communication: the tag employs the radar clutter as a carrier signal to load a data message, while the reader aims to decode the message sent by the tag in the presence of the interference (clutter) generated by the radar transmitter.

## II. SYSTEM DESCRIPTION AND MODEL DEVELOPMENT

We consider the ambient backscatter communication system in Fig. 1. Here, a radar transmitter illuminates a given region, and passive scatterers yield a reverberation towards both the tag and the reader. The tag exploits the incident clutter as an ambient carrier to send a message to the reader. The radar emits the passband signal  $\Re\{a(t)e^{i2\pi f_a t}\}$ , where  $f_a$  is the carrier frequency and  $a(t)$  is a baseband periodic waveform of period  $T_a$  and bandwidth  $W_a$ , so that the radar delay resolution is  $1/W_a$  [24]. For a non-scanning (pulsed or continuous-wave) radar,  $T_a$  is the period of the modulating signal or a multiple thereof; instead, for a scanning radar, it is the scan-time or a multiple thereof. The knowledge of  $a(t)$  is not needed in the following developments.

### A. Signal emitted by the tag

Let  $\Re\{c(t)e^{i2\pi f_a t}\}$  be the radar clutter hitting the tag, including the possible direct signal from the radar to the tag, where  $c(t)$  is its baseband representation; then, we have

$$c(t) = \int_{-\infty}^{\infty} \gamma(t, \tau) a(t - \tau) d\tau \quad (1)$$

where  $\gamma(t, \tau)$  is the unknown baseband impulse response of the radar-tag channel. We assume that the coherence time of  $\gamma(t, \tau)$  spans several, say  $L_a$ , radar periods, so that  $c(t)$  is a *locally periodic* signal: this means that  $c(t)$  presents  $L_a$  approximately-equal cycles within any time segment of length  $L_a T_a$ , as a consequence of the periodic structure of the radar excitation. For a stationary scenario,  $\gamma(t, \tau) = \gamma(\tau)$ , and  $c(t)$  is itself periodic with period  $T_a$ .

The tag modulates the RF signal  $\Re\{c(t)e^{i2\pi f_a t}\}$  to send a message  $s(t)$  [19]; in particular, the backscatter modulator alters this incident waveform by switching the antenna load between two or

more states (thus changing its phase and/or amplitude) every symbol interval  $T_s = T_a/N_a$ , where  $N_a$  is the number of symbols sent over one radar period. We denote by  $x_{p,n}$  the  $n$ -th symbol in the  $p$ -th radar period;  $x_{p,n}$  specifies the complex reflection coefficient of the antenna load employed during the time interval  $[(pN_a + n)T_s, (pN_a + n + 1)T_s]$ , for  $p \in \mathbb{Z}$  and  $n = 0, \dots, N_a - 1$ , and belongs to a given discrete alphabet containing the possible reflection coefficients allowed by the available hardware (more on this in Sec. III). The baseband representation of the RF signal backscattered by the tag can be written as<sup>1</sup>

$$x(t) = c(t) \underbrace{\sum_{p \in \mathbb{Z}} \sum_{n=0}^{N_a-1} x_{p,n} \Pi \left( \frac{t - (pN_a + n)T_s}{\Delta_s} \right)}_{s(t)} = \sum_{p \in \mathbb{Z}} \sum_{n=0}^{N_a-1} x_{p,n} \underbrace{c(t) \Pi \left( \frac{t - (pN_a + n)T_s}{\Delta_s} \right)}_{\phi_{p,n}(t)} \quad (2)$$

where  $\Pi(t/\Delta_s)$  is a rectangular pulse with unit amplitude, support  $[0, \Delta_s]$ , and bandwidth  $W_s = 1/\Delta_s$ . We assume that  $T_s = \Delta_s + \Delta_g$ , where  $\Delta_g$  is a guard interval between two consecutive transmissions (more on this in Sec. II-B). For the reader's sake, a graphical description of  $c(t)$ ,  $s(t)$ , and  $x(t)$  is reported in Fig. 2. The following remarks are now in order.

*Remark 1.* The tag performs a temporal gating of the ambient carrier through a switch commuting between the transmit and silent states and loads the symbol  $x_{p,n}$  on the pulse  $\phi_{p,n}(t)$ . The tag has no information on the radar signal and no control on the environmental response. What matters here is that, since  $c(t)$  is a locally periodic signal,  $\phi_{p,n}(t - mT_a) \simeq \phi_{p+m,n}(t)$  for  $m = 0, \dots, L_a - 1$ , whereby two symbols spaced up  $mN_a$  positions apart can be assumed to modulate the same (even though unknown) pulse: see Fig. 2(c) for a graphical description.  $\square$

*Remark 2.* If  $\Delta_s > 1/W_a$ , the transmission of  $x_{p,n}$  occurs over a time interval larger than the delay resolution of the radar; in this case, the pulse  $\phi_{p,n}(t)$  may result from the linear superposition of multiple echoes with resolvable delays that hit the tag over the time interval  $[(pN_a + n)T_s, (pN_a + n)T_s + \Delta_s]$ ; accordingly, its values may significantly change during the transmission of  $x_{p,n}$ . If  $\Delta_s < 1/W_a$ , we can instead write

$$x(t) \simeq \sum_{p \in \mathbb{Z}} \sum_{n=0}^{N_a-1} x_{p,n} \underbrace{c((pN_a + n)T_s) \Pi \left( \frac{t - (pN_a + n)T_s}{\Delta_s} \right)}_{\phi_{p,n}(t)} \quad (3)$$

<sup>1</sup>We neglect the internal thermal noise of the tag, as its circuits consist only of passive components [25].

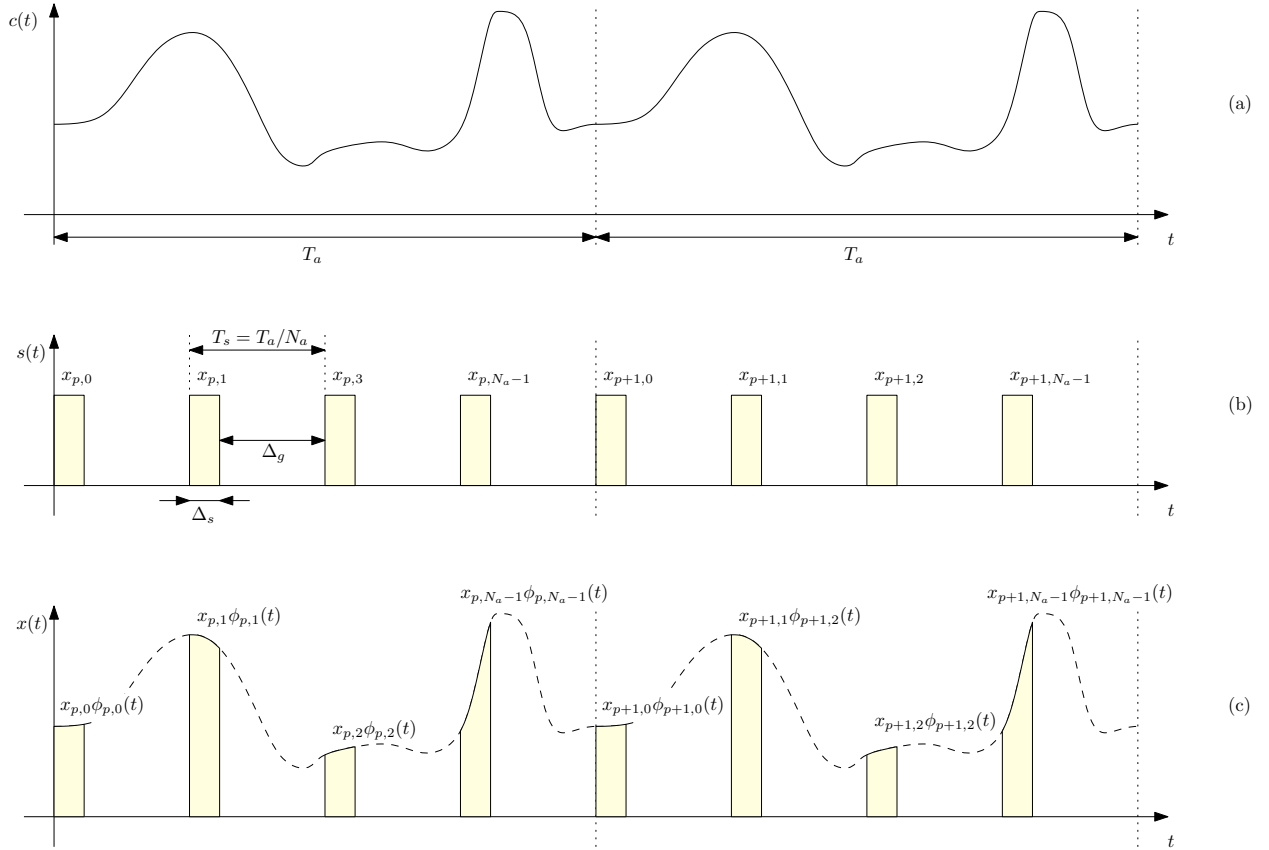


Figure 2. (a) Radar clutter  $c(t)$  employed by the tag as an ambient carrier over two radar periods when  $L_a \geq 2$ . (b) Message  $s(t)$  sent by the tag. (c) Modulated signal  $x(t)$  back-scattered by the tag.

whereby the pulse  $\phi_{p,n}(t)$  approximately maintains an unknown constant amplitude  $c((pN_a + n)T_s)$  during the transmission of  $x_{p,n}$ ; if  $T_s \ll 1/W_a$ , the value of  $c((pN_a + n)T_s)$  may even remain approximately constant over few consecutive transmissions.  $\square$

*Remark 3.* The alphabet of the tag and the parameters  $N_a$ ,  $\Delta_s$ , and  $\Delta_g$  are under the designer's control. For example, reducing the number  $N_a$  of symbols per radar period may allow to increase the duration  $\Delta_s$  of each modulated pulse and therefore its energy, thus extending the communication range; also, if the tag needs to harvest energy when not transmitting, the duration of the guard interval can be increased by either increasing the symbol interval  $T_s$  and/or decreasing the pulse duration  $\Delta_s$ . For low-cost and power-limited devices, an alphabet with small cardinality can be used to simplify the hardware and reduce the power consumption [19]. If instead the tag has access to a power source and is equipped with a more advanced hardware (possibly including an active amplifier), then a larger alphabet can be employed; in particular, tags

equipped with reconfigurable intelligent surfaces (RISs) may implement combined modulation and passive beamforming [26], [27].  $\square$

### B. Signal received by the reader

If the reader knows the radar carrier frequency, its baseband received signal can be written as

$$\tilde{y}(t) = \beta x(t - \tau) + i(t) + \omega(t) \quad (4)$$

where  $\tau \geq 0$  is the propagation delay between the tag and the reader,  $\beta \in \mathbb{C}$  is the unknown attenuation in the tag-reader channel (including the scattering efficiency of the tag and any carrier phase offset),  $i(t)$  is the unknown interference (i.e., the baseband representation of the radar clutter hitting the reader), and  $\omega(t)$  is the thermal noise, which is modeled as a white complex Gaussian process with power spectral density  $\sigma_\omega^2$ . Even though  $c(t)$  and  $i(t)$  are produced by the environment in response to the same radar excitation, they are in general different, since tag and reader are in different locations (whereby an echo generated by the same object may arrive with a different delay and/or amplitude) and their antennas have a different orientation and radiation pattern (whereby they may observe echoes originated from different objects). We assume that the coherence time of the radar-reader channel spans  $L_a$  radar periods, so that  $i(t)$  is also locally periodic over any time segment of length  $L_a T_a$ .

The signal in (4) is passed through a unit-energy low-pass filter  $\psi(t)$ , which has bandwidth  $W_\psi$  and support in  $[0, \Delta_\psi]$ , with  $\Delta_\psi \leq \Delta_g$ , whose output is

$$y(t) = \tilde{y}(t) \star \psi(t) = \underbrace{\sum_{p \in \mathbb{Z}} \sum_{n=0}^{N_a-1} x_{p,n} \underbrace{\beta \phi_{p,n}(t - \tau) \star \psi(t)}_{\alpha_{p,n}(t - \tau)}}_{\beta x(t - \tau) \star \psi(t)} + i(t) \star \psi(t) + \omega(t) \star \psi(t). \quad (5)$$

In the previous equation,  $\alpha_{p,n}(t - \tau)$  is the unknown received pulse carrying the symbol  $x_{p,n}$ , which accounts for the radar clutter  $\phi_{p,n}(t - \tau)$  hitting the tag in the time interval  $[(pN_a + n)T_s, (pN_a + n)T_s + \Delta_s]$ , the attenuation  $\beta$  of the tag-reader channel, and the receive filter  $\psi(t)$  of the reader. The assumption  $\Delta_\psi \leq \Delta_g$  implies that  $\Delta_s + \Delta_\psi \leq T_s$ ; accordingly, there is no intersymbol interference in the filtered received signal  $r(t)$ ; to better illustrate this point, we provide in Fig. 3a a graphical description of the waveform  $\beta x(t - \tau) \star \psi(t)$ : it is seen that the received pulses  $\{\alpha_{p,n}(t - \tau)\}$  do not overlap in time.

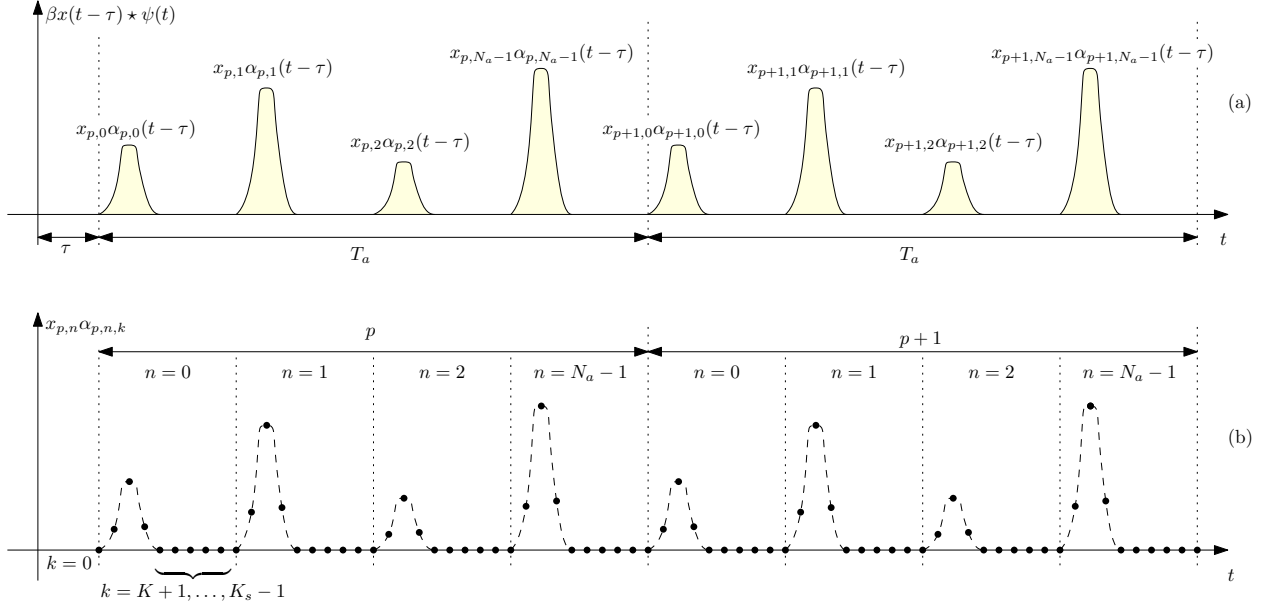


Figure 3. Example of the waveform  $\beta x(t - \tau) \star \psi(t)$  at the output of the receive filter over two radar periods (a) and of the corresponding samples (b) when  $L_a \geq 2$ ,  $N_a = 4$ ,  $K = 3$ , and  $K_s = 9$ .

The signal  $r(t)$  is sampled at rate  $K_s/T_s$ , where  $K_s \in \mathbb{N}$  is a design parameter; accordingly, the sample taken at the epoch  $\tau + pT_a + nT_s + kT_s/K_s$  is

$$\begin{aligned}
 y_{p,n,k} &= r(t) \star \psi(t) \Big|_{t=\tau+pT_a+nT_s+kT_s/K_s} \\
 &= x_{p,n} \underbrace{\alpha_{p,n}(t - \tau) \Big|_{t=\tau+pT_a+nT_s+kT_s/K_s}}_{\alpha_{p,n,k}} \\
 &\quad + \underbrace{i(t) \star \psi(t) \Big|_{t=\tau+pT_a+nT_s+kT_s/K_s}}_{i_{p,n,k}} + \underbrace{\omega(t) \star \psi(t) \Big|_{t=\tau+pT_a+nT_s+kT_s/K_s}}_{\omega_{p,n,k}} \\
 &= x_{p,n} \alpha_{p,n,k} + i_{p,n,k} + \omega_{p,n,k}
 \end{aligned} \tag{6}$$

for  $p \in \mathbb{Z}$ ,  $n = 0, \dots, N_a - 1$ , and  $k = 0, \dots, K_s - 1$ . Fig. 3b provides an illustration of the samples of the waveform  $\beta x(t - \tau) \star \psi(t)$  in Fig. 3a. The following remarks are now given.

*Remark 4.* To reject the out-of-band noise and preserve the signal of interest, the bandwidth  $W_\psi$  of the receive filter should equal the bandwidth  $W_x \simeq W_a + W_s$  of the modulated signal  $x(t)$ . Also, to avoid information loss in the discretization process,  $K_s \in \mathbb{N}$  should be at least equal to  $\lceil W_\psi T_s \rceil$ . Needless to say, lower values of  $W_\psi$  and/or  $K_s$  can be employed to reduce the implementation complexity at the price of some loss.  $\square$

*Remark 5.* The correlation between the noise samples  $\omega_{p_1, n_1, k_1}$  and  $\omega_{p_2, n_2, k_2}$  is

$$\mathbb{E} [\omega_{p_1, n_1, k_1} \omega_{p_2, n_2, k_2}^*] = \sigma_\omega^2 R_\psi \left( (p_1 - p_2)T_a + (n_1 - n_2)T_s + (k_1 - k_2)T_s/K_s \right) \quad (7)$$

where  $R_\psi(t) = \psi(t) \star \psi^*(-t)$  is the autocorrelation function of  $\psi(t)$ . Since  $R_\psi(t)$  has support  $[0, 2\Delta_\psi]$ , the above statistical expectation is zero if  $p_1 \neq p_2$  or  $n_1 \neq n_2$  or  $|k_1 - k_2|T_s/K_s \geq 2\Delta_\psi$ ; for  $p_1 = p_2$ ,  $n_1 = n_2$ ,  $k_1 \neq k_2$ , and  $|k_1 - k_2|T_s/K_s < 2\Delta_\psi$ , the corresponding samples are uncorrelated only if  $R_\psi(\ell T_s/K_s) = 0$  for  $|\ell| = 1, \dots, \lceil 2\Delta_\psi K_s/T_s \rceil - 1$ . For example, this is the case when  $\psi(t) = \sqrt{K_s/T_s} \Pi(tK_s/T_s)$ . For simplicity, hereafter we assume that the received filter is designed to have uncorrelated noise samples.  $\square$

*Remark 6.* Due to the presence of the guard intervals, we have

$$\alpha_{p, n, k} = 0, \quad \text{if } k = 0 \text{ or } k = K + 1, \dots, K_s \quad (8)$$

where  $K = \lceil (\Delta_s + \Delta_\psi)K_s/T_s \rceil - 1$ . Hence, only the samples  $r_{p, n, 1}, \dots, r_{p, n, K}$  contain the signal of interest in the time interval  $[\tau + (pN_a + n)T_s, \tau + (pN_a + n + 1)T_s]$ , as also shown in Fig. 3b: in the following, we only process such data samples and ignore the others.  $\square$

*Remark 7.* For any  $n$  and  $k$ , the sequences  $\{\alpha_{p, n, k}\}_{p \in \mathbb{Z}}$  and  $\{i_{p, n, k}\}_{p \in \mathbb{Z}}$  contain samples of the waveforms  $\sum_{p \in \mathbb{Z}} \alpha_{p, n}(t - \tau)$  and  $i(t)$ , respectively, which are spaced one radar period apart. The local periodicity of  $c(t)$  and  $i(t)$  implies that both these sequences are *locally constant*, i.e., that  $L_a$  consecutive elements are approximately equal.  $\square$

### III. ENCODING/DECODING STRATEGIES

We propose here encoding/decoding schemes relying only on prior knowledge of the radar period and of the coherence time of the radar-tag-reader and radar-reader channels. To proceed, we parse the received data samples in (6) into  $N_a$  groups, which define as many time-orthogonal subchannels; in particular, the  $n$ -th subchannel contains the observations  $\{r_{p, n, 1}, \dots, r_{p, n, K}\}_{p \in \mathbb{Z}}$  taken in the  $n$ -th symbol interval of each radar period  $p \in \mathbb{Z}$ , for  $n = 0, \dots, N_a - 1$ . This is motivated by the fact that, according to Remark 7, the samples  $\alpha_{p, n, 1}, \dots, \alpha_{p, n, K}$  of the pulse carrying the symbol  $x_{p, n}$  and the corresponding samples  $i_{p, n, 1}, \dots, i_{p, n, K}$  of the radar interference remain approximately constant in up to  $L_a$  consecutive uses of the  $n$ -th subchannel (i.e.,  $L_a$  consecutive radar periods). To take advantage of such memory, we consider disjoint blocks of  $L$  consecutive subchannel uses (hereafter referred to as frames), where  $L \leq L_a$  is a design parameter tied to the affordable system complexity. The  $\ell$ -th frame spans the radar periods

indexed by  $\ell L, \dots, (\ell + 1)L - 1$ , with  $\ell \in \mathbb{Z}$ , and the reader is aware of the beginning of each frame. In the  $\ell$ -th frame, the received data samples of the  $n$ -th subchannels can be organized into the following matrix

$$\mathbf{Y}_n(\ell) = \begin{bmatrix} y_{\ell L, n, 1} & \cdots & y_{\ell L, n, K} \\ \vdots & & \vdots \\ y_{(\ell+1)L-1, n, 1} & \cdots & y_{(\ell+1)L-1, n, K} \end{bmatrix} \in \mathbb{C}^{L \times K}. \quad (9)$$

The entries in each row of  $\mathbf{Y}_n(\ell)$  correspond to time epochs spaced  $T_s/K_s$  apart within the same radar period (fast-time, in the radar jargon) and contain the same symbol. Instead, the entries in each column of  $\mathbf{Y}_n(\ell)$  correspond to time epochs spaced one radar period apart within the same frame (slow-time, in the radar jargon), so that we can assume here that they share the same value of the carrier signal and radar interference, i.e.,

$$\alpha_{\ell L, n, k} = \cdots = \alpha_{(\ell+1)L-1, n, k} \quad (10a)$$

$$i_{\ell L, n, k} = \cdots = i_{(\ell+1)L-1, n, k} \quad (10b)$$

for  $k = 1, \dots, K$ . Hence, upon defining

$$\boldsymbol{\alpha}_n(\ell) = [\alpha_{\ell L, n, 1} \cdots \alpha_{\ell L, n, K}]^T \in \mathbb{C}^K \quad (11a)$$

$$\mathbf{i}_n(\ell) = [i_{\ell L, n, 1} \cdots i_{\ell L, n, K}]^T \in \mathbb{C}^K \quad (11b)$$

$$\mathbf{x}_n(\ell) = [x_{\ell L, n} \cdots x_{(\ell+1)L-1, n}]^T \in \mathcal{X}^L \quad (11c)$$

we can write

$$\mathbf{Y}_n(\ell) = \mathbf{x}_n(\ell) \boldsymbol{\alpha}_n^T(\ell) + \mathbf{1}_L \mathbf{i}_n^T(\ell) + \boldsymbol{\Omega}_n(\ell) \quad (12)$$

where the noise matrix  $\boldsymbol{\Omega}_n(\ell) \in \mathbb{C}^{L \times K}$  is defined similarly to  $\mathbf{Y}_n(\ell)$  and its entries are independent circularly-symmetric Gaussian random variables with variance  $\sigma_w^2$ . See Fig. 4 for a graphical description.

The quality of the  $N_a$  subchannels may be different, as they may be sustained by different radar echoes; hence, the tag may decide to use only those experiencing a strong enough ambient carrier. Two strategies are proposed next to use any given subchannel, which rely upon frame-by-frame and frame-differential encoding, respectively; also, we show that joint coding among multiple subchannels is possible and that multiple tags can be accommodated on the same subchannel.

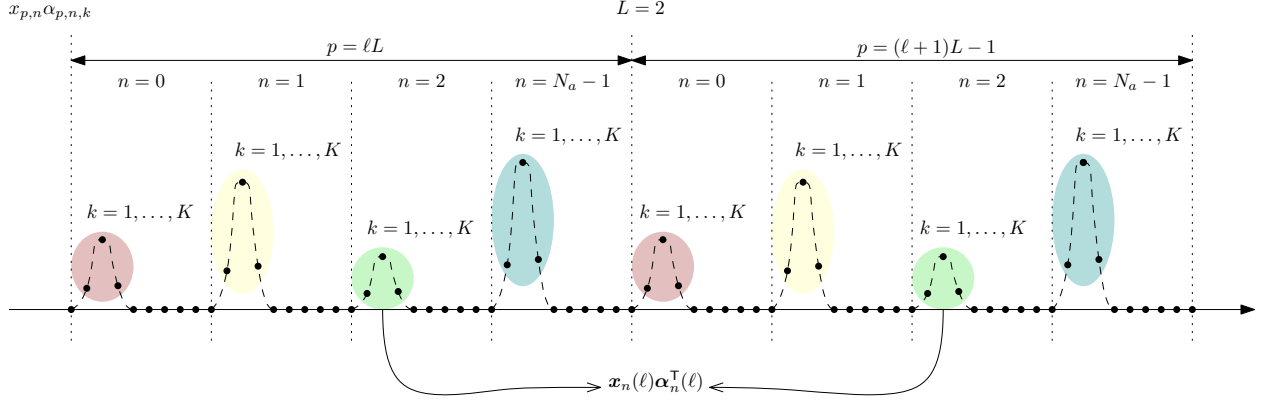


Figure 4. We consider here a frame spanning  $L = 2$  radar periods, with  $N_a = 4$ ,  $K = 3$ , and  $K_s = 9$ , and reports the samples of the waveform  $\beta x(t - \tau) \star \psi(t)$  given in Fig. 3. Only the non-zero samples corresponding to  $k = 1, \dots, K$  are processed; in particular, such samples are parsed in  $N_a$  groups. Each group corresponds to a different subchannel.

### A. Frame-by-frame encoding

Consider a given subchannel and frame; for convenience, we drop here the subchannel index  $n$  and the frame index  $\ell$ , whereby the received signal in (12) becomes

$$\mathbf{Y} = \mathbf{x}\boldsymbol{\alpha}^\top + \mathbf{1}_L \mathbf{i}^\top + \boldsymbol{\Omega}. \quad (13)$$

If the codeword  $\mathbf{x}$  is drawn from a codebook  $\mathcal{U} \subseteq \mathbb{C}^L$ , then the resulting transmission rate is

$$R = \frac{1}{L} \log_2 |\mathcal{U}| \quad [\text{bits/subchannel-use}]. \quad (14)$$

Notice that the transmission of any codeword  $\mathbf{u} = (u_1 \cdots u_L)^\top \in \mathcal{U}$  is accomplished by using the reflection coefficients  $u_1, \dots, u_L$  in  $L$  consecutive subchannel uses; accordingly, the alphabet (i.e., the set of possible reflection coefficients) employed by the tag is  $\mathcal{X} = \bigcup_{\mathbf{u} \in \mathcal{U}} \bigcup_{j=1}^L \{u_j\}$ .

The reader is faced with the problem of estimating the codeword  $\mathbf{x} \in \mathcal{U}$  when both  $\boldsymbol{\alpha}$  and  $\mathbf{i}$  are unknown and treated as nuisance parameters. It is shown in Appendix A that the maximum likelihood (ML) estimator of  $\mathbf{x}$  is

$$\hat{\mathbf{x}} = \arg \max_{\mathbf{u} \in \mathcal{U}} \frac{\|\mathbf{u}^\top \mathbf{P} \mathbf{Y}\|^2}{\|\mathbf{P} \mathbf{u}\|^2} \quad (15)$$

where

$$\mathbf{P} = \mathbf{I}_L - \frac{1}{L} \mathbf{1}_L \mathbf{1}_L^\top \quad (16)$$

is the projector onto the orthogonal complement of the subspace spanned by the radar interference. When the decoding rule in (15) is employed, any fraction of power allocated in the

subspace spanned by the interference is wasted, as a consequence of the multiplication of  $\mathbf{Y}$  by  $\mathbf{P}$ ; furthermore, any two codewords  $\mathbf{u}, \mathbf{z} \in \mathcal{U}$  such that  $\mathbf{P}\mathbf{u} \propto \mathbf{P}\mathbf{z}$  cannot be distinguished, as a consequence of the fact that the channel state  $\boldsymbol{\alpha}$  is unknown. Accordingly, it is desirable to choose a codebook  $\mathcal{U}$  possessing the following properties

$$(P1) \quad \mathbf{u}^H \mathbf{1}_L = 0 \text{ for any } \mathbf{u} \in \mathcal{U}$$

$$(P2) \quad \text{Rank}\{[\mathbf{P}\mathbf{u} \quad \mathbf{P}\mathbf{z}]\} = 2 \text{ for any } \mathbf{u}, \mathbf{z} \in \mathcal{U} \text{ and } \mathbf{u} \neq \mathbf{z}$$

to make the most of the available energy, while keeping all of the codewords distinguishable in the absence of noise. Hereafter, we assume that both (P1) and (P2) hold, which implies  $L \geq 3$  if<sup>2</sup>  $|\mathcal{U}| \geq 2$ ; accordingly, the decoding rule in (15) reduces to

$$\hat{\mathbf{x}} = \arg \max_{\mathbf{u} \in \mathcal{U}} \frac{\|\mathbf{u}^H \mathbf{Y}\|^2}{\|\mathbf{u}\|^2} \quad (17)$$

so that the interference-free direction (i.e., the codeword) in  $\mathcal{U}$  containing the largest portion of the received energy is selected; the rule in (17) further simplifies to

$$\hat{\mathbf{x}} = \arg \max_{\mathbf{u} \in \mathcal{U}} \|\mathbf{u}^H \mathbf{Y}\|^2. \quad (18)$$

if all the codewords have the same energy. We discuss next two relevant examples.

*Example 1* (Orthogonal codewords). A practical option is to choose a codebook containing orthogonal codewords with equal energy. Without loss of generality, assume that  $\|\mathbf{u}\|^2 = L$  for any  $\mathbf{u} \in \mathcal{U}$ . In this case, condition (P1) implies that  $|\mathcal{U}| \leq L - 1$ , while the decision statistic in (18) takes the form

$$\mathbf{u}^H \mathbf{Y} = \begin{cases} L\boldsymbol{\alpha}^T + \mathbf{w}^T, & \text{if } \mathbf{x} = \mathbf{u} \\ \mathbf{w}^T, & \text{otherwise} \end{cases} \quad (19)$$

where  $\mathbf{w}^T = \mathbf{u}^H \boldsymbol{\Omega}$  is a complex circularly-symmetric Gaussian vector with covariance matrix  $L\sigma_w^2 \mathbf{I}_K$ . It is seen that this encoding/decoding strategy is able to get rid of the radar interference and achieve a coherent integration gain of  $L$ . Also, upon exploiting the fact that

$$\frac{2}{L\sigma_w^2} \|\mathbf{u}_j^H \mathbf{Y}\|^2 \sim \begin{cases} \chi_{2K}^2(2L\|\boldsymbol{\alpha}\|^2/\sigma_w^2), & \text{if } j = i \\ \chi_{2K}^2, & \text{otherwise} \end{cases} \quad (20)$$

if  $\mathbf{x} = \mathbf{u}_i$  is sent, it can be verified that the error probability conditioned upon  $\boldsymbol{\alpha}$  is

$$P(e | \boldsymbol{\alpha}) = 1 - \int_0^\infty \left( 1 - e^{-x/2} \sum_{k=0}^{K-1} \frac{(x/2)^k}{k!} \right)^{|\mathcal{U}|-1} \frac{1}{2} e^{-(x+2L\|\boldsymbol{\alpha}\|^2/\sigma_w^2)/2}$$

<sup>2</sup>In Sec. III-B, we may also allow  $|\mathcal{U}| = 1$ ; in this case only (P1) need to be satisfied, which implies  $L \geq 2$ .

$$\times \left( \frac{x}{2L\|\boldsymbol{\alpha}\|^2/\sigma_w^2} \right)^{(K-1)/2} I_{K-1} \left( \sqrt{2L\|\boldsymbol{\alpha}\|^2} x / \sigma_w^2 \right) dx. \quad (21)$$

For  $K = 1$ , the expression in (21) simplifies to the well known formula

$$P(e | \boldsymbol{\alpha}) = \sum_{k=1}^{|\mathcal{U}|-1} \frac{(-1)^{k+1}}{k+1} \binom{|\mathcal{U}|-1}{k} e^{-\frac{k}{k+1} \frac{2L\|\boldsymbol{\alpha}\|^2}{2\sigma_w^2}} \quad (22)$$

that is the error probability of orthogonal signaling with non-coherent detection [28]. If  $L$  is a power of 2, a possible choice for  $\mathcal{U}$  are the columns (except  $\mathbf{1}_L$ ) of the Hadamard matrix of order  $L$ , so that  $\mathcal{X} = \{-1, 1\}$ , and only 2 phase states are needed at the tag.  $\square$

*Example 2* ( $M$ -PSK alphabet). If the entries of the codewords in  $\mathcal{U}$  are taken from the  $M$ -PSK alphabet  $\{e^{i2\pi m/M}\}_{m=0}^{M-1}$ , then we have  $\mathcal{X} = \{e^{i2\pi m/M}\}_{m=0}^{M-1}$ , and only  $M$  phase states are needed at the tag. Tables I and II show the number of codewords, the transmission rate (in bits/subchannel-use) and the worst-case cosine similarity among the codewords

$$\max_{\substack{\mathbf{u}, \mathbf{z} \in \mathcal{U} \\ \mathbf{u} \neq \mathbf{z}}} \frac{|\mathbf{u}^H \mathbf{z}|}{\|\mathbf{u}\| \|\mathbf{z}\|} \quad (23)$$

for the largest codebook satisfying (P1) and (P2). Only non-trivial designs with at least two codewords are shown. For  $M > 2$ , the above quantities have been obtained via an exhaustive search. For  $M = 2$ , instead, it can be shown that (P1) and (P2) implies that  $L$  must be even and limits the number of codewords to  $\frac{1}{2} \binom{L}{L/2}$ ; in this case, the transmission rate is  $R = \frac{1}{L} \log_2 \left( \frac{1}{2} \binom{L}{L/2} \right)$ , the worst-case cosine similarity is<sup>3</sup>  $|1 - 4/L|$ , and both increase with  $L$ . For comparison, Tables I and II also analyze the relevant case where the additional constraint that the codewords be mutually orthogonal is enforced; in this case, the transmission rate obtained with the largest possible codebook inevitably converges to zero with an increasing  $L$ .  $\square$

### B. Frame-differential encoding

A major limitation of the signaling scheme in Sec. III-A is the shortage of low-correlated codewords satisfying conditions (P1) and (P2); in particular, the number of orthogonal messages is inherently limited by the chosen frame length  $L$ . When  $L \leq L_a/2$ , we can overcome this drawback by resorting to a more elaborated signaling scheme which includes a differential encoding over two consecutive frames.

<sup>3</sup>This result follows from the facts that, in (23),  $\|\mathbf{u}\| = \|\mathbf{z}\| = \sqrt{L}$ ,  $|\mathbf{u}^H \mathbf{z}| = \left| \sum_{i=1}^L u_i z_i \right| = |2\delta - L| \leq L - 4$ , where  $\delta$  is the number of positions in which  $u_i = z_i$ , and equality holds if  $\delta = 2$  or  $\delta = L - 2$ .

Table I

NUMBER OF CODEWORDS, TRANSMISSION RATE (IN BITS/SUBCHANNEL-USE) AND WORST-CASE COSINE SIMILARITY AMONG THE CODEWORDS FOR THE LARGEST CODEBOOK SATISFYING (P1) AND (P2) WHEN A 2-PSK ALPHABET IS USED

$L$	No. codewords		Rate		Similarity	
	non-orth.	orth.	non-orth.	orth.	non-orth.	orth.
4	3	3	0.3962	0.3962	0	0
6	10	–	0.5537	–	0.3333	–
8	35	7	0.6412	0.3509	0.5000	0
10	126	–	0.6977	–	0.6000	–
12	462	11	0.7907	0.2883	0.6667	0
14	1716	–	0.7675	–	0.7143	–
16	6435	15	0.7729	0.2442	0.7500	0
18	24310	–	0.8094	–	0.7778	–

To proceed, we consider a given subchannel; for convenience, we drop the subchannel index  $n$ , whereby the received signal in (12) becomes

$$\mathbf{Y}(\ell) = \mathbf{x}(\ell)\boldsymbol{\alpha}^T(\ell) + \mathbf{1}_L \mathbf{i}^T(\ell) + \boldsymbol{\Omega}(\ell). \quad (24)$$

The tag sends the message  $\mathbf{x}(\ell) = b(\ell)\mathbf{u}(\ell)$ , where  $\mathbf{u}(\ell) \in \mathcal{U}$ , and  $\{b(\ell)\}_{\ell \in \mathbb{Z}}$  is a sequence of differentially encoded  $M$ -PSK symbols, with  $M \geq 2$ . In this case, the alphabet used by the tag is  $\mathcal{X} = \bigcup_{m=0}^{M-1} \bigcup_{\mathbf{u} \in \mathcal{U}} \bigcup_{j=1}^L \{e^{i2\pi m/M} u_j\}$ , while the transmission rate is

$$R = (\log_2 |\mathcal{U}| + \log_2 M) / L \quad [\text{bits/subchannel-use}]. \quad (25)$$

Let  $\theta(\ell)$  denote the incremental phase shift in the differential encoding, i.e.,  $b(\ell) = e^{i\theta(\ell)} b(\ell-1)$ , and consider the observable  $\mathbf{Y}(\ell)$  and  $\mathbf{Y}(\ell-1)$  collected in two subsequent frames. Then, since  $\boldsymbol{\alpha}(\ell) = \boldsymbol{\alpha}(\ell-1)$  and  $\mathbf{i}(\ell) = \mathbf{i}(\ell-1)$ , the ML estimate of  $(\theta(\ell), \mathbf{u}(\ell))$  based on  $\mathbf{Y}(\ell)$  and  $\mathbf{Y}(\ell-1)$  takes the following form

$$\begin{aligned} (\hat{\theta}(\ell), \hat{\mathbf{u}}(\ell)) &= \arg \max_{\theta \in \{2\pi m/M\}_{m=0}^{M-1}} \max_{\substack{\mathbf{z} \in \mathcal{U} \\ \mathbf{u} \in \mathcal{U}}} \left\| \begin{bmatrix} e^{i\theta} \mathbf{u} \\ \mathbf{z} \end{bmatrix}^H \begin{bmatrix} \mathbf{Y}(\ell) \\ \mathbf{Y}(\ell-1) \end{bmatrix} \right\|^2 \\ &= \arg \max_{\theta \in \{2\pi m/M\}_{m=0}^{M-1}} \max_{\substack{\mathbf{z} \in \mathcal{U} \\ \mathbf{u} \in \mathcal{U}}} \left\| e^{-i\theta} \mathbf{u}^H \mathbf{Y}(\ell) + \mathbf{z}^H \mathbf{Y}(\ell-1) \right\|^2. \end{aligned} \quad (26)$$

Table II  
NUMBER OF CODEWORDS, TRANSMISSION RATE (IN BITS/SUBCHANNEL-USE) AND WORST-CASE COSINE SIMILARITY  
AMONG THE CODEWORDS FOR THE LARGEST CODEBOOK SATISFYING (P1) AND (P2) WHEN AN  $M$ -PSK ALPHABET IS  
USED

$M$	$L$	No. codewords		Rate		Similarity	
		non-orth.	orth.	non-orth.	orth.	non-orth.	orth.
3	3	2	2	0.3333	0.3333	0.6667	0
	6	30	5	0.8178	0.3870	0.8333	0
	4	9	3	0.7925	0.3962	0.7500	0
4	6	100	5	1.1073	0.3870	0.8333	0
	8	1225	7	1.2823	0.3509	0.8750	0
	5	24	4	0.9170	0.4	0.8000	0
5	3	2	2	0.3333	0.3333	0.6667	0
	4	15	3	0.9767	0.3962	0.8660	0
	5	60	—	1.1814	—	0.8718	—
	6	340	5	1.4016	0.3870	0.8819	0
	7	1680	6	1.5306	0.3693	0.8921	0
	8	9135	7	1.6446	0.3509	0.9014	0

Notice that a search over a set of cardinality  $M|\mathcal{U}|^2$  is required in (26). To reduce the decoding complexity, we can replace the nuisance parameter  $\mathbf{u}(\ell-1)$  by its estimate, say  $\hat{\mathbf{u}}'(\ell-1)$ , obtained in the previous frame; in this case, the decoding rule is

$$\{\hat{\theta}'(\ell), \hat{\mathbf{u}}'(\ell)\} = \arg \max_{\substack{\theta \in \{2\pi m/M\}_{m=0}^{M-1} \\ \mathbf{u} \in \mathcal{U}}} \left\| e^{-i\theta} \mathbf{u}^H \mathbf{Y}(\ell) + (\hat{\mathbf{u}}'(\ell-1))^H \mathbf{Y}(\ell-1) \right\|^2 \quad (27)$$

which requires a search over a set of cardinality  $M|\mathcal{U}|$ . An even simpler decoding rule is obtained by relaxing the grid  $\{2\pi m/M\}_{m=0}^{M-1}$  to the continuous interval  $[0, 2\pi]$  and, then, projecting the relaxed solution onto the original search set; in this case, we have

$$\hat{\mathbf{u}}_{\text{sub}}(\ell) = \arg \max_{\mathbf{u} \in \mathcal{U}} \left\| \mathbf{v}^H \mathbf{Y}(\ell) \right\|^2 \quad (28a)$$

$$\hat{\theta}_{\text{sub}}(\ell) = \arg \min_{\theta \in \{2\pi m/M\}_{m=0}^{M-1}} \left| \theta - \angle(\hat{\mathbf{u}}_{\text{sub}}^H(\ell) \mathbf{Y}(\ell) \mathbf{Y}^H(\ell-1) \hat{\mathbf{u}}_{\text{sub}}(\ell-1)) \right| \quad (28b)$$

so that the reader first recovers  $\mathbf{u}(\ell)$  from (28a), and then accomplishes differential decoding with (28b) by considering the statistic  $\hat{\mathbf{u}}_{\text{sub}}^H(\ell) \mathbf{Y}(\ell) \mathbf{Y}^H(\ell-1) \hat{\mathbf{u}}_{\text{sub}}(\ell-1)$ .

*Example 3* (Combined orthogonal/differential encoding). A simple scheme is obtained when the set  $\mathcal{U}$  contains mutually-orthogonal and equal energy codewords, as in Example 1. When a binary differential encoding is adopted, then the possible messages are  $\{\mathbf{u}, -\mathbf{u}\}_{\mathbf{u} \in \mathcal{U}}$ . Also, if  $M$  is a power of 2 and the entries of the codewords in  $\mathcal{U}$  are also taken from an  $M$ -PSK alphabet, then only  $M$  phase states are needed at the tag.  $\square$

*Example 4* (Combined repetition/differential encoding). Another practical option is to choose  $\mathcal{U} = \{\mathbf{u}\}$ , so that the tag sends the message  $\mathbf{x}(\ell) = b(\ell)\mathbf{u}$ , where  $\mathbf{u}$  is any vector orthogonal to  $\mathbf{1}_L$ : this means that the same differentially-encoded symbol  $b(\ell)$  is repeated in all radar periods of the frame. In this case, the ML decoding rule in (26) becomes

$$\hat{\theta}(\ell) = \arg \min_{\theta \in \{2\pi m/M\}_{m=0}^{M-1}} \left| \theta - \angle(\mathbf{u}^H \mathbf{Y}(\ell) \mathbf{Y}^H(\ell-1) \mathbf{u}) \right|. \quad (29)$$

Remarkably, if  $M$  and  $L$  are even and  $\mathbf{u}$  is a vector with half entries equal to 1 and the other half equal to  $-1$ , only  $M$  phase states are needed at the tag. Also, notice that the error probability is available in closed-form for  $K = 1$  [28]: it is the error probability of the  $M$ -ary differential phase shift keying modulation; in particular, we have

$$P(e | \alpha(\ell)) = \frac{1}{\pi} \int_0^{\pi - \pi/M} e^{-\frac{\sin^2(\pi/M)}{1 + \cos(\pi/M) \cos \theta} \frac{L|\alpha(\ell)|^2}{\sigma_w^2}} d\theta$$

$$\begin{cases} = \frac{1}{2} e^{-L|\alpha(\ell)|^2/\sigma_w^2}, & \text{if } M = 2 \\ \approx 2Q\left(\sqrt{\frac{L|\alpha(\ell)|^2}{\sigma_w^2} \sin^2(\pi/M)}\right), & \text{if } M > 2 \text{ and } L|\alpha(\ell)|^2 \gg \sigma_w^2 \end{cases} \quad (30)$$

where  $Q(x) = \int_x^\infty \frac{1}{\sqrt{2\pi}} e^{-t^2/2} dt$ .  $\square$

### C. Encoding across subchannels

It is worthwhile to notice that encoding across  $B \geq 2$  subchannels can be also performed. Let  $n_1, \dots, n_B$  denote the indexes of such subchannels; we only discuss next two simple examples, deferring to future studies a more in depth analysis.

*Example 5* (Repetition encoding). The same message is repeated here over the  $B$  subchannels, so that  $\bar{\mathbf{x}}(\ell) = \mathbf{x}_{n_1}(\ell) = \dots = \mathbf{x}_{n_B}(\ell)$ . In this case, we can arrange the corresponding received samples in each frame  $\ell$  as follows

$$\begin{aligned} \bar{\mathbf{Y}}(\ell) &= \begin{bmatrix} \mathbf{Y}_{n_1}(\ell) & \dots & \mathbf{Y}_{n_B}(\ell) \end{bmatrix} \\ &= \bar{\mathbf{x}}(\ell) \bar{\boldsymbol{\alpha}}^T(\ell) + \mathbf{1}_L \bar{\mathbf{i}}^T(\ell) + \bar{\boldsymbol{\Omega}}(\ell) \in \mathbb{C}^{L \times BK} \end{aligned} \quad (31)$$

where  $\bar{\boldsymbol{\alpha}}(\ell) = [\boldsymbol{\alpha}_{n_1}^\top(\ell) \cdots \boldsymbol{\alpha}_{n_B}^\top(\ell)]^\top$ ,  $\bar{\mathbf{i}}(\ell) = [\mathbf{i}_{n_1}^\top(\ell) \cdots \mathbf{i}_{n_B}^\top(\ell)]^\top$ , and  $\bar{\boldsymbol{\Omega}}(\ell) = [\boldsymbol{\Omega}_{n_1}(\ell) \cdots \boldsymbol{\Omega}_{n_B}(\ell)]$ . The signaling strategies illustrated in the Secs. III-A and III-B can be directly applied to the input/output model in (31). Pros and cons here are evident: indeed, an energy and, possibly, a diversity gain can be obtained at the price of a rate loss. Accordingly, this strategy may be helpful when the considered subchannels are sustained by weak or fluctuating echoes.  $\square$

*Example 6* (Subchannels with equal clutter). Assume to have  $B$  adjacent subchannels experiencing the same carrier signal and radar interference, so that  $\bar{\boldsymbol{\alpha}}(\ell) = \boldsymbol{\alpha}_{n_1}(\ell) = \cdots = \boldsymbol{\alpha}_{n_B}(\ell)$  and  $\bar{\mathbf{i}}(\ell) = \mathbf{i}_{n_1}(\ell) = \cdots = \mathbf{i}_{n_B}(\ell)$ . This occurs when  $BT_s$  is much smaller than the radar delay resolution. In this case, we can arrange the received samples as

$$\begin{aligned} \bar{\mathbf{Y}}(\ell) &= \left[ \mathbf{Y}_{n_1}^\top(\ell) \cdots \mathbf{Y}_{n_B}^\top(\ell) \right]^\top \\ &= \bar{\mathbf{x}}(\ell) \bar{\boldsymbol{\alpha}}^\top(\ell) + \mathbf{1}_L \bar{\mathbf{i}}^\top(\ell) + \bar{\boldsymbol{\Omega}}(\ell) \in \mathbb{C}^{BL \times K} \end{aligned} \quad (32)$$

where  $\bar{\mathbf{x}}(\ell) = [\mathbf{x}_{n_1}^\top(\ell) \cdots \mathbf{x}_{n_B}^\top(\ell)]^\top$  and  $\bar{\boldsymbol{\Omega}}(\ell) = [\boldsymbol{\Omega}_{n_1}^\top(\ell) \cdots \boldsymbol{\Omega}_{n_B}^\top(\ell)]^\top$ . Again, the signaling strategies illustrated in Secs. III-A and III-B can be directly applied to the input/output model in (32). The main advantage here is that communication can take place even when  $L = 1$  by making the bandwidth of the modulated signal much larger than that of the radar excitation.  $\square$

#### IV. MULTIPLE TAGS

The above signaling schemes can be generalized to serve multiple synchronous tags on the same subchannel. For brevity, we only consider here frame-by-frame encoding.

##### A. Sourced multiple access

Consider first a sourced multiple access with  $Q$  active tags; in this case, the reader is interested in both the received messages and the identities of the tags that generated them. The model in (13) is modified as follows

$$\mathbf{Y} = \sum_{q=1}^Q \mathbf{x}^{(q)} (\boldsymbol{\alpha}^{(q)})^\top + \mathbf{1}_L \mathbf{i}^\top + \boldsymbol{\Omega} = \mathbf{X}^{(1:Q)} (\mathbf{A}^{(1:Q)})^\top + \mathbf{1}_L \mathbf{i} + \boldsymbol{\Omega} \quad (33)$$

where  $\mathbf{x}^{(q)} \in \mathcal{U}^{(q)}$  is the codeword sent by the tag  $q$ ,  $\mathcal{U}^{(q)}$  is the codebook employed by the tag  $q$ ,  $\boldsymbol{\alpha}^{(q)}$  contains the samples of the pulse carrying the symbols in  $\mathbf{x}^{(q)}$ ,  $\mathbf{X}^{(1:Q)} = [\mathbf{x}^{(1)} \cdots \mathbf{x}^{(Q)}]$ , and  $\mathbf{A}^{(1:Q)} = [\boldsymbol{\alpha}^{(1)} \cdots \boldsymbol{\alpha}^{(Q)}]$ . As shown in Appendix A, the ML decoding rule is now

$$\hat{\mathbf{X}}^{(1:Q)} = \arg \max_{\mathbf{U} \in \mathcal{U}_s^{(1:Q)}} \left\| \mathbf{P}\mathbf{U}(\mathbf{P}\mathbf{U})^\dagger \mathbf{P}\mathbf{Y} \right\|_F^2 \quad (34)$$

where  $\mathbf{P}$  is given in (16),  $\mathbf{P}\mathbf{U}(\mathbf{P}\mathbf{U})^\dagger$  is the orthogonal projector on the column space of the matrix  $\mathbf{P}\mathbf{U}$ , and

$$\mathcal{U}_s^{(1:Q)} = \left\{ [\mathbf{u}^{(1)} \ \dots \ \mathbf{u}^{(Q)}] : \mathbf{u}^{(q)} \in \mathcal{U}^{(q)} \ \forall q \right\}. \quad (35)$$

When the decoding rule in (34) is employed, any fraction of power allocated in the subspace spanned by the interference is wasted; also, the matrices  $\mathbf{U}, \mathbf{Z} \in \mathcal{U}_s^{(1:Q)}$  cannot be distinguished if  $\mathbf{P}\mathbf{U}$  and  $\mathbf{P}\mathbf{Z}$  present the same column span, while  $\mathbf{U}$  will always be preferred to  $\mathbf{Z}$  if the column span of  $\mathbf{P}\mathbf{Z}$  is strictly contained in that of  $\mathbf{P}\mathbf{U}$ . Accordingly, it is desirable that the adopted codebooks  $\mathcal{U}^{(1)}, \dots, \mathcal{U}^{(Q)}$  possess the following properties

$$(P1s) \ \mathbf{U}^H \mathbf{1}_L = \mathbf{0}_Q \text{ for any } \mathbf{U} \in \mathcal{U}_s^{(1:Q)}$$

$$(P2s) \ \text{Rank}\{\mathbf{P}\mathbf{U}\} = Q \text{ and } \text{Rank}\{\mathbf{P}\mathbf{U} \ \mathbf{P}\mathbf{Z}\} \geq Q + 1 \text{ for any } \mathbf{U}, \mathbf{Z} \in \mathcal{U}_s^{(1:Q)} \text{ and } \mathbf{U} \neq \mathbf{Z}$$

which generalize those given in Section III-A; in particular, these properties ensure that the identities of the tags and their messages are identifiable in the absence of noise and imply  $L \geq Q + 2$ . In this case, the decoding rule in (34) simplifies to

$$\hat{\mathbf{X}}^{(1:Q)} = \arg \max_{\mathbf{U} \in \mathcal{U}_s^{(1:Q)}} \|\mathbf{U}\mathbf{U}^\dagger \mathbf{Y}_n(\ell)\|_F^2. \quad (36)$$

To avoid the joint search among the  $Q$  tags in (36), we may suboptimally use a standard orthogonal matching pursuit (OMP) [29], which is summarized in Algorithm 1. In this case, one tag at the time is iteratively decoded. In each iteration, the codeword with the largest contribution to the residual signal  $\mathbf{Z}$ , as measured by the norm of the inner product with  $\mathbf{Z}$ , is added to the set of detected codewords. Once a codeword belonging to tag  $m_j$  is detected, its codebook  $\mathcal{U}^{(m_j)}$  is excluded from the search space in subsequent iterations (see step 5). The current set of detected codewords form the columns of a matrix  $\hat{\mathbf{X}}$  and the residual is computed by subtracting from  $\mathbf{Y}$  the projection of  $\mathbf{Y}$  onto  $\hat{\mathbf{X}}$ 's column space. The complexity of Algorithm 1 is dominated by the pseudoinverse in step 7 and therefore is  $\mathcal{O}(QL^3)$ .

### B. Unsourced multiple access

Consider now an unsourced multiple access where  $Q_{\max}$  active tags employ the same codebook  $\mathcal{U}$ . In this case, the reader is interested only in the received messages, while the identities of the tags that generated them is irrelevant [30]. The number  $Q$  of distinct messages received by the

---

**Algorithm 1** Orthogonal Matching Pursuit (sourced)

---

- 1:  $\mathcal{M} = \{1, \dots, Q\}$ ,  $\mathbf{Z} = \mathbf{Y}$
  - 2: **for**  $j = 1, \dots, Q$  **do**
  - 3:    $m_j = \arg \max_{q \in \mathcal{M}} \max_{\mathbf{u} \in \mathcal{U}^{(q)}} \|\mathbf{u}^H \mathbf{Z}\|^2$
  - 4:    $\hat{\mathbf{x}}^{(m_j)} = \arg \max_{\mathbf{u} \in \mathcal{U}^{(m_j)}} \|\mathbf{u}^H \mathbf{Z}\|^2$
  - 5:    $\mathcal{M} = \mathcal{M} \setminus \{m_j\}$
  - 6:    $\hat{\mathbf{X}} = [\hat{\mathbf{x}}^{(m_1)} \dots \hat{\mathbf{x}}^{(m_j)}]$
  - 7:    $\mathbf{Z} = (\mathbf{I}_L - \hat{\mathbf{X}} \hat{\mathbf{X}}^\dagger) \mathbf{Y}$
  - 8: **end for**
  - 9: **return**  $\hat{\mathbf{x}}^{(1)}, \dots, \hat{\mathbf{x}}^{(Q)}$
- 

reader may now be lower than the number of active tags, as more tags may transmit the same codeword; accordingly, the resulting average transmission rate per each tag is<sup>4</sup>

$$R = \frac{1}{LQ_{\max}} \mathbb{E} \left[ \sum_{q=0}^{Q-1} \log_2(|\mathcal{U}| - q) \right] \quad [\text{bits/subchannel-use/tag}]. \quad (38)$$

where the expectation is taken over the random variable  $Q \in \{1, \dots, Q_{\max}\}$ . Let  $\mathcal{H}_Q$  be the hypothesis that  $Q$  distinct messages are selected, for  $Q = 1, \dots, Q_{\max}$ . Under  $\mathcal{H}_Q$ , the received signal can be still expressed as in (33) with  $\mathbf{X}^{(1:Q)} \in \mathcal{U}_u^{(1:Q)}$ , where

$$\mathcal{U}_u^{(1:Q)} = \{[\mathbf{u}^{(1)} \dots \mathbf{u}^{(Q)}] : \mathbf{u}^{(q)} \in \mathcal{U} \forall q \text{ and } \mathbf{u}^{(i)} \neq \mathbf{u}^{(j)} \forall i \neq j\}. \quad (39)$$

By the same arguments illustrated before, it is desirable that  $\mathcal{U}$  satisfies (P1) given in Sec. III-A; also, in the absence of noise, the identifiability of the messages under  $\mathcal{H}_Q$  is possible if

$$\text{(P2u)} \quad \text{Rank}\{\mathbf{U}\} = Q \text{ and } \text{Rank}\{[\mathbf{U} \mathbf{Z}]\} \geq Q + 1 \text{ for any } \mathbf{U}, \mathbf{Z} \in \mathcal{U}_u^{(1:Q)} \text{ and } \mathbf{U} \neq \mathbf{Z}.$$

<sup>4</sup>Assume for example that  $Q_{\max} = 2$  and that each tag randomly selects a codeword from  $|\mathcal{U}|$ . If the tags select the same codeword, which occurs with probability  $1/|\mathcal{U}|$ , the received message conveys  $\log_2 |\mathcal{U}|$  bits in  $L$  subchannel uses; if instead the tags select distinct codewords, which occurs with probability  $(|\mathcal{U}| - 1)/|\mathcal{U}|$ , the two received messages convey  $\log_2 |\mathcal{U}| + \log_2 (|\mathcal{U}| - 1)$  bits in  $L$  subchannel uses. Accordingly, we have

$$R = \frac{1}{2L|\mathcal{U}|} \log_2 |\mathcal{U}| + \frac{|\mathcal{U}| - 1}{2L|\mathcal{U}| (\log_2 |\mathcal{U}| + \log_2 (|\mathcal{U}| - 1))}. \quad (37)$$

---

**Algorithm 2** Orthogonal Matching Pursuit (unsourced)
 

---

- 1: Given number of tags  $Q_{\max}$ , shared codebook  $\mathcal{U}$ , threshold  $\eta$
  - 2:  $\hat{Q} = 0$ ,  $\mathbf{Z} = \mathbf{Y}$
  - 3: **for**  $j = 1, \dots, Q_{\max}$  **do**
  - 4:    $\hat{Q} = \hat{Q} + 1$
  - 5:    $\hat{\mathbf{x}}^{(j)} = \arg \max_{\mathbf{u} \in \mathcal{U}} \|\mathbf{u}^H \mathbf{Z}\|^2$
  - 6:    $\hat{\mathbf{X}} = [\hat{\mathbf{x}}^{(1)} \dots \hat{\mathbf{x}}^{(j)}]$
  - 7:    $\mathbf{Z} = (\mathbf{I}_L - \hat{\mathbf{X}} \hat{\mathbf{X}}^\dagger) \mathbf{Y}$
  - 8:   **if**  $\|\mathbf{Z}\|_F < \eta$  **then**
  - 9:     **break**
  - 10:   **end if**
  - 11: **end for**
  - 12: **return**  $\hat{\mathbf{x}}^{(1)}, \dots, \hat{\mathbf{x}}^{(\hat{Q})}$
- 

In this case, upon resorting to a generalized information criterion (GIC), an estimate  $\hat{Q}$  of the number of messages is [11], [31]

$$\hat{Q} = \arg \max_{Q \in \{1, \dots, Q_{\max}\}} \left\{ \max_{\mathbf{U} \in \mathcal{U}_u^{(1:Q)}} \|\mathbf{U} \mathbf{U}^\dagger \mathbf{Y}_n(\ell)\|_F^2 - \gamma Q \right\} \quad (40)$$

where  $\gamma$  is a convenient penalty factor. For a given  $\hat{Q}$ , the ML estimate of the messages is

$$\hat{\mathbf{X}}^{(1:\hat{Q})} = \arg \max_{\mathbf{U} \in \mathcal{U}_u^{(1:\hat{Q})}} \|\mathbf{U} \mathbf{U}^\dagger \mathbf{Y}_n(\ell)\|_F^2. \quad (41)$$

Alternatively, we may resort to an adaptive version of Algorithm 1, which extracts the superimposed back-scattered messages one-by-one [11]: for the reader's sake, Algorithm 2 summarizes this OMP-based procedure.

## V. PERFORMANCE ANALYSIS

In this section we provide some examples to assess the performance of the proposed signaling schemes and illustrate some relevant system tradeoffs. Following [32], the samples of the radar clutter are modelled as noncentral chi-square random variables in the considered subchannel; also, they remain constant over a frame and then independently change from frame to frame, thus resulting into a block fading channel model. More specifically, we assume in (12) that  $\boldsymbol{\alpha}_n(\ell) = \boldsymbol{\alpha}_{s,n}(\ell) + \boldsymbol{\alpha}_{d,n}(\ell)$ , where  $\boldsymbol{\alpha}_{s,n}(\ell)$  and  $\boldsymbol{\alpha}_{d,n}(\ell)$  represent the specular (deterministic)

and diffuse (random) components, respectively. The entries of  $\alpha_{s,n}(\ell)$  have the same magnitude  $\sigma_{s,\alpha} > 0$ ; instead,  $\alpha_{d,n}(\ell)$  is a complex circularly-symmetric Gaussian random vector with covariance matrix  $\mathbf{C} \in \mathbb{C}^{K \times K}$ ; the entries of  $\mathbf{C}$  are modeled as  $[\mathbf{C}]_{ij} = \rho^{|i-j|} \sigma_{d,\alpha}^2$  for some  $\rho \in [0, 1]$  and  $\sigma_{d,\alpha}^2 > 0$ . Notice here that  $\kappa_\alpha = \sigma_{s,\alpha}^2 / \sigma_{d,\alpha}^2$  is the power ratio between the specular and diffuse component; also,  $(\sigma_{s,\alpha}^2 + \sigma_{d,\alpha}^2) / \sigma_w^2$  is the received signal-to-noise (SNR); finally,  $\rho$  rules the covariance among the entries of  $\alpha_n(\ell)$ ; in particular, sampling the received signal at the Nyquist rate may produce low- or highly-correlated entries if  $\Delta_s \gg 1/W_a$  or  $\Delta_s \ll 1/W_a$ , respectively (see also Remark 2). Unless otherwise stated, we assume  $\kappa_\alpha = 1/9$ ,  $\rho = 0$ ,  $L = 8$ , and  $K = 2$ . Finally, the codewords are assumed equally probable, and the system performance is assessed in terms of  $P(e)$ , i.e., the probability that a message is erroneously decoded by the reader, which is computed by averaging over  $10^6$  channel realizations.

#### A. Frame-by-frame encoding

We consider here the signaling strategy discussed in Sec. III-A. The codebook  $\mathcal{U}$  adopted in (13) satisfies both (P1) and (P2), with the entries of all codewords taken from a 2-PSK alphabet. The feasible designs for  $L \leq 18$  are listed in Table I; for example,  $\mathcal{U}$  can contain up to 35 codewords when  $L = 8$ , with at most 7 mutually-orthogonal codewords corresponding to the columns of the  $8 \times 8$  Hadamard matrix, except the all-one vector.

We first assume that  $\mathcal{U}$  contains 4 mutually-orthogonal codewords and study the impact of  $K$ ,  $\rho$ ,  $\kappa$ , and  $L$ . Fig. 5 shows  $P(e)$  versus SNR for  $K = 2, 3, 4$  and  $\rho = 0, 1$ ; it is seen that increasing  $K$  (i.e., the duration  $\Delta_s$  of each transmitted pulse for a fixed radar bandwidth and sampling rate) provides an SNR gain, as a longer segment of the radar clutter hitting the tag is exploited to convey each symbol; for  $\rho = 0$ , a diversity gain  $K$  is also obtained, as we have  $K$  uncorrelated clutter samples. Fig. 6 shows  $P(e)$  versus SNR for  $\kappa_\alpha = 1/9, 1, 9$  and  $L = 8, 16$ ;  $P(e)$  decreases with  $\kappa_\alpha$ , as a stronger specular component is present; also, there is an integration gain of 3 dB when  $L$  is doubled at the price of a rate loss, in keeping with Example 1.

Finally, Fig. 7 shows  $P(e)$  versus the transmission rate, for SNR = 0, 5, 10 dB and  $L = 6, 8$ . Here, the codebook size is varied from 2 to 10 for  $L = 6$  and from 2 to 35 for  $L = 8$ , according to Table I; for an increasing size, the codebook is augmented by first including the mutually-orthogonal codewords (when they exist) and then the non-orthogonal ones. It is verified that  $P(e)$  gracefully degrades as the transmission rate increases; also, more favorable tradeoffs are obtained with a larger value of  $L$ .

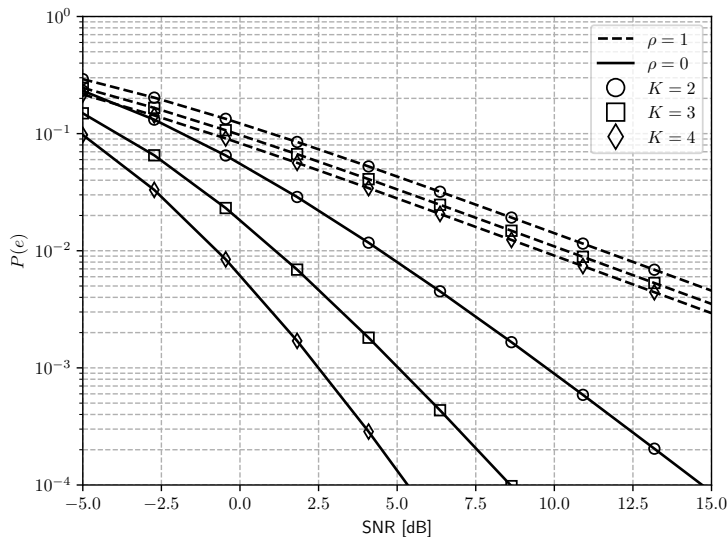


Figure 5.  $P(e)$  versus SNR for  $K = 2, 3, 4$  and  $\rho = 0, 1$ , when  $L = 8$ ,  $\kappa_\alpha = 1/9$ , the frame-by-frame encoding strategy in Sec. III-A is employed, and the codebook contains 4 mutually-orthogonal codewords (therefore, the transmission rate is 0.25 bits/subchannel-use).

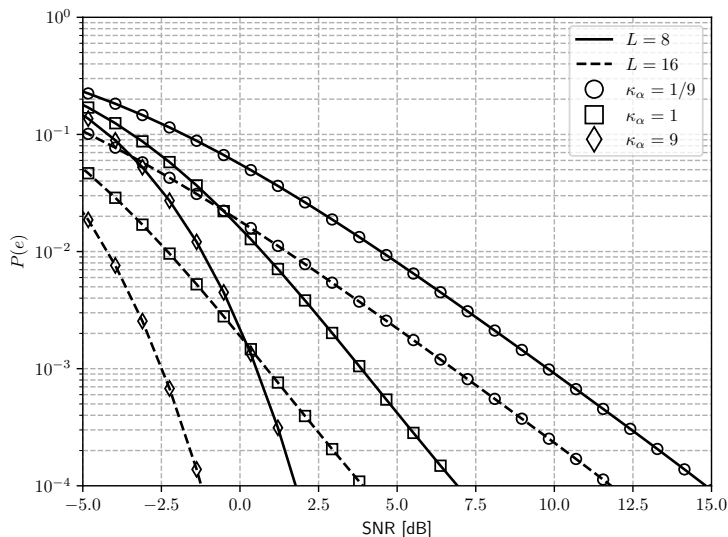


Figure 6.  $P(e)$  versus SNR for  $\kappa_\alpha = 1/9, 1, 9$  and  $L = 8, 16$ , when  $K = 2$ ,  $\rho = 0$ , the frame-by-frame encoding strategy in Sec. III-A is employed, and the adopted codebook contains 4 mutually-orthogonal codewords (therefore, the transmission rate is 0.25 bits/subchannel-use).

### B. Frame-differential encoding

We consider here the signaling strategy discussed in Sec. III-B; the set  $\mathcal{U}$  adopted in (24) is constructed as in Sec. V-A. In Fig. 8, we first compare the decoding rules in (26), (27), and (28),

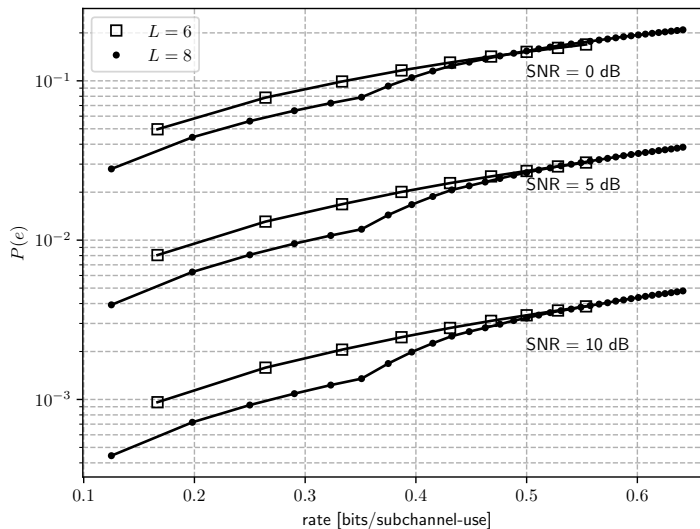


Figure 7.  $P(e)$  versus the transmission rate for SNR = 0, 5, 10 dB and  $L = 6, 8$ , when  $K = 2$ ,  $\rho = 0$ ,  $\kappa_\alpha = 1/9$ , and the frame-by-frame encoding strategy in Sec. III-A is employed.

when  $M = 2, 4, 8$  and  $\mathcal{U}$  contains 4 mutually-orthogonal codewords. It is seen that the first two rules provide a similar error probability; also, the rule in (28) is only slightly inferior with respect to the former two and, therefore, can be preferred in practice to reduce complexity.

Next, we compare frame-differential and frame-by-frame encoding, when the same frame length and binary alphabet are employed. Fig. 9 shows  $P(e)$  versus SNR when  $D/L$  bits per subchannel-use are sent by the tag, for  $D = 1, 3, 5$ : this is obtained with  $M = 2$  and  $|\mathcal{U}| = 2^{D-1}$  for frame-differential encoding and  $|\mathcal{U}| = 2^D$  for frame-by-frame encoding. Also, Fig. 10 shows  $P(e)$  versus the transmission rate, for SNR = 0, 5, 10 dB. For frame-differential encoding, we only consider the decoding rules in (26) and (28). It is verified that frame-differential encoding provides a lower error probability for the same transmission rate; also, it can sustain larger transmission rates. This result indicates that the rate-splitting across the codebook  $\mathcal{U}$  and the differential-encoded phase offset is advantageous, as it reduces the similarity among the messages. More generally, notice that the available degrees of freedom to get a desired transmission rate are the number of frames  $L$ , the size  $M$  of the PSK constellation adopted for differential-encoding, and the codebook  $\mathcal{U}$ , which in principle may be jointly optimized to obtain a desired link quality and alphabet: this challenging problem is left for future studies.

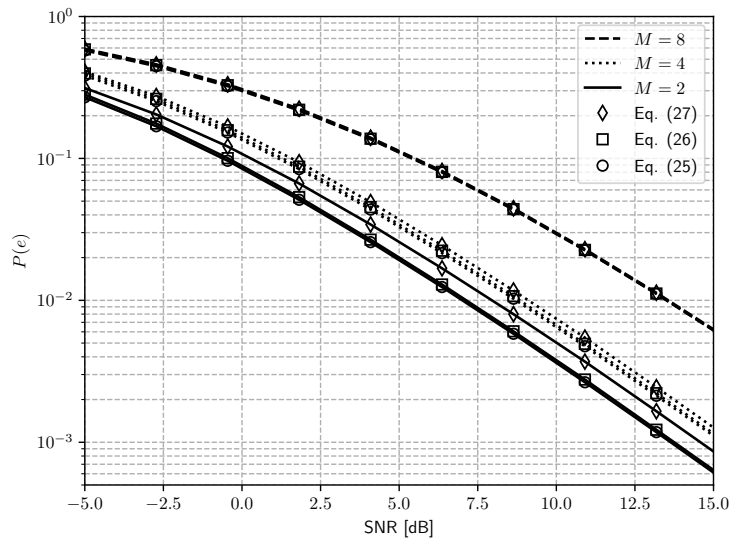


Figure 8.  $P(e)$  versus SNR for  $M = 2, 4, 8$ , when  $L = 8$ ,  $K = 2$ ,  $\rho = 0$ ,  $\kappa_\alpha = 1/9$ , the frame-differential encoding strategy in Sec. III-B is employed and  $\mathcal{U}$  contains 4 mutually-orthogonal codewords (therefore, the transmission rate is 0.375, 0.5, 0.625 bits/subchannel-use for  $M = 2, 8$ , respectively).

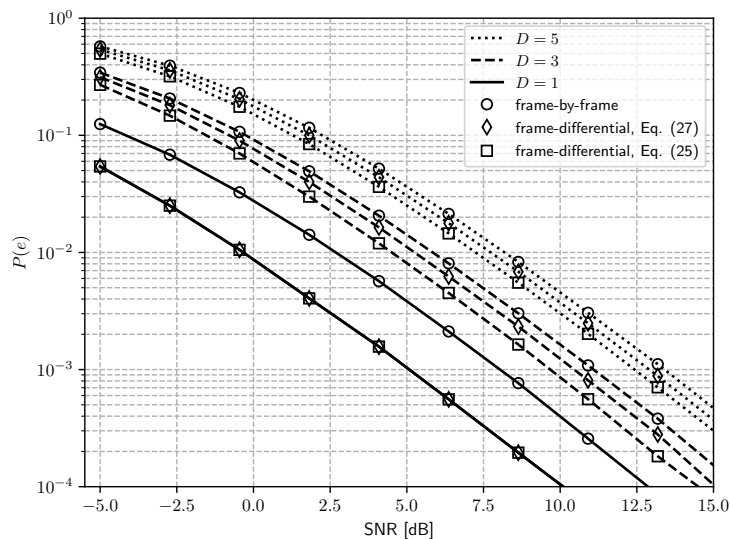


Figure 9.  $P(e)$  versus SNR when  $L = 8$ ,  $K = 2$ ,  $\rho = 0$ , and  $\kappa_\alpha = 1/9$ . The transmission rate is  $D/L$  bits per subchannel-use, for  $D = 1, 3, 5$ . For frame-differential encoding,  $M = 2$  and  $|\mathcal{U}| = 2^{D-1}$ ; for frame-by-frame encoding,  $|\mathcal{U}| = 2^D$ .

### C. Multiple tags

Finally, we consider the scenario discussed in Sec. IV, when two active tags are present and the entries of all codewords are taken from a 2-PSK alphabet. Fig. 11 shows  $P(e)$  (averaged over all tags) versus the transmission rate of each tag for both a sourced and an unsourced

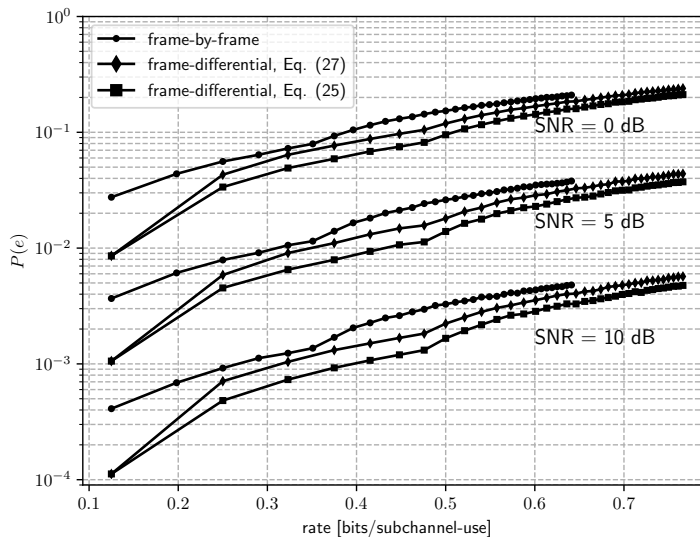


Figure 10.  $P(e)$  versus the transmission rate for SNR = 0, 5, 10 dB, when  $L = 8$ ,  $K = 2$ ,  $\rho = 0$ ,  $\kappa_\alpha = 1/9$ . For frame-differential encoding,  $M = 2$  and  $|\mathcal{U}|$  is varied from 1 to 35; for frame-by-frame encoding,  $|\mathcal{U}|$  is varied from 2 to 35.

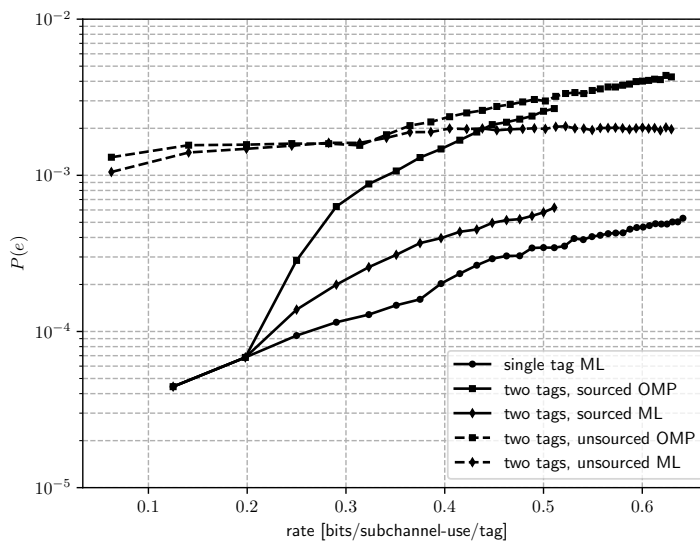


Figure 11.  $P(e)$  (averaged over all tags) versus the transmission rate of each tag, when 1 or 2 tags are present, SNR = 15 dB,  $L = 8$ ,  $K = 2$ ,  $\rho = 0$ , and  $\kappa_\alpha = 1/9$ . Both a sourced and an unsourced multiple access is considered with ML or OMP-based decoding, as discussed in Sec. IV.

multiple access, when SNR = 15 dB and either ML or OMP-based decoding is employed; for comparison, the performance obtained with a single tag is also included (see also Fig. 7).

For a sourced multiple access, the largest codebooks  $\mathcal{U}^{(1)}$  and  $\mathcal{U}^{(2)}$  satisfying (P1s) and (P2s) have  $|\mathcal{U}^{(1)}| = |\mathcal{U}^{(2)}| = 17$ ; hence, the curve for  $Q = 2$  ends at  $(\log_2 17)/8 = 0.5109$

bits/subchannel-use/tag. When the transmission rate is  $1/L$  or  $(\log_2 3)/L$  bits/subchannel-use/tag,  $P(e)$  is the same for  $Q = 1, 2$ , as mutually-orthogonal codewords are assigned here to all tags. For larger transmission rates, this orthogonality condition cannot be ensured anymore, and multiple tags can be accommodated only at the price of increasing  $P(e)$ ; in this operating regime, ML decoding is superior to OMP-based decoding, as it can better handle the multi-tag interference.

For an unsourced multiple access, the largest shared codebook  $\mathcal{U}$  satisfying (P1) and (P2u) has  $|\mathcal{U}| = 35$ , as in the single-tag case. As expected, this multiple access strategy suffers a larger error probability than the sourced counterpart, as both the number of distinct messages and their content must be jointly estimated; however, it can support larger transmission rates.

## VI. CONCLUSIONS

In this work, we have put forwards the idea that the radar clutter can be used as a carrier signal to enable an ambient backscatter communication. We have presented the signal model describing this system architecture and highlighted the interplay among the main system parameters. Upon exploiting the periodic structure of the radar clutter over time scales shorter than the channel coherence time we have derived encoding/decoding strategies which allow the reader to distinguish the message sent by the one or multiple tags from the superimposed radar interference without requiring a coordination with the radar transmitter or the knowledge of the radar waveform and of the radar-tag-reader and radar-reader channels.

The potential applications of this form of ambient backscatter communication are many. For example, a multitude of low-cost tags deployed in the region covered by a surveillance radar (either indoor or outdoor) can form a power-efficient network and exchange data with no additional electromagnetic emission. Likewise, a car equipped with a collocated radar and reader may receive data from tags deployed on other cars or on the side of the road while scanning for prospective obstacles. The radar and the ambient backscatterers may be even collaborative devices of the same network; in this case, the radar transmitter may intentionally query/activate nearby tags by forming directional beams towards them and gather information about the environment.

Future study should explore more sophisticated signaling schemes and multiple access protocols, also to support massive machine type communications. Also, the Doppler effect and the imperfect synchronism between the tag and the reader or among the multiple tags should be accounted for at both the design and the analysis stage. Finally, the use of reconfigurable

intelligent surfaces may greatly expand the potentiality of this idea by enlarging the coverage area and limiting the signal leakage towards undesired directions.

## APPENDIX A

### PROOF OF (15) AND (34)

Here we derive the ML decoding rule in (34) for the observation model in (33): when  $Q = 1$ , we have  $\mathbf{X}^{(1:Q)} = \mathbf{x}$ ,  $\mathbf{A}^{(1:Q)} = \boldsymbol{\alpha}$ , and  $\mathcal{U}_s^{(1:Q)} = \mathcal{U}$ , so that the model in (33) reduces to that in (13), and (34) simplifies to (15). To simplify the notation, we drop the subscripts in (33) and write the received signal as  $\mathbf{Y} = \mathbf{X}\mathbf{A}^\top + \mathbf{1}_L \mathbf{i}^\top + \boldsymbol{\Omega}$ . Accordingly, the ML estimator of  $\mathbf{X}$  is

$$\hat{\mathbf{X}} = \arg \min_{\mathbf{X} \in \mathcal{U}_s^{(1:Q)}} \min_{\mathbf{A} \in \mathbb{C}^{K \times Q}, \mathbf{i} \in \mathbb{C}^L} \|\mathbf{Y} - \mathbf{X}\mathbf{A}^\top - \mathbf{1}_L \mathbf{i}^\top\|_F^2 \quad (42)$$

where  $\mathcal{U}_s^{(1:Q)}$  is the set in (35). Notice now that

$$\begin{aligned} \|\mathbf{Y} - \mathbf{X}\mathbf{A}^\top - \mathbf{1}_L \mathbf{i}^\top\|_F^2 &= \text{Tr}(\mathbf{Y}\mathbf{Y}^\text{H}) + \text{Tr}(\mathbf{X}\mathbf{A}^\top \mathbf{A}^* \mathbf{X}^\text{H}) + L\|\mathbf{i}\|^2 \\ &\quad - 2\Re\{\mathbf{X}^\text{H}\mathbf{Y}\mathbf{A}^* + \mathbf{1}_L^\top \mathbf{Y}\mathbf{i}^* - \mathbf{1}_L^\top \mathbf{X}\mathbf{A}^\top \mathbf{i}^*\} \end{aligned} \quad (43)$$

and the conditions for the minimum over  $(\boldsymbol{\alpha}, \mathbf{i})$  are

$$L\mathbf{i} = \mathbf{Y}^\top \mathbf{1}_L - \mathbf{A}\mathbf{X}^\top \mathbf{1}_L \quad (44a)$$

$$\mathbf{A}\mathbf{X}^\top \mathbf{X}^* = \mathbf{Y}^\top \mathbf{X}^* - \mathbf{i}\mathbf{1}_L^\top \mathbf{X}^*. \quad (44b)$$

Eliminating  $\mathbf{i}$  in (44b), we get

$$\hat{\mathbf{A}}(\mathbf{X}) = ((\mathbf{X}^\text{H}\mathbf{P}\mathbf{X})^\dagger \mathbf{X}^\text{H}\mathbf{P}\mathbf{Y})^\top \quad (45)$$

where  $\mathbf{P}$  is the orthogonal projector in (16), and, plugging (45) in (44a), we obtain

$$\hat{\mathbf{i}}(\mathbf{X}) = \frac{1}{L} (\mathbf{1}^\top (\mathbf{I}_L - \mathbf{X}(\mathbf{X}^\text{H}\mathbf{P}\mathbf{X})^\dagger \mathbf{X}^\text{H}\mathbf{P}) \mathbf{Y})^\top. \quad (46)$$

Finally, we have

$$\begin{aligned} \hat{\mathbf{X}} &= \arg \min_{\mathbf{X} \in \mathcal{U}_s^{(1:Q)}} \|\mathbf{Y} - \mathbf{X}\hat{\mathbf{A}}^\top(\mathbf{X}) - \mathbf{1}_L \hat{\mathbf{i}}^\top(\mathbf{X})\|_F^2 \\ &= \arg \min_{\mathbf{X} \in \mathcal{U}_s^{(1:Q)}} \|\mathbf{P}\mathbf{Y} - \mathbf{P}\mathbf{X}(\mathbf{X}^\text{H}\mathbf{P}\mathbf{X})^\dagger \mathbf{X}^\text{H}\mathbf{P}\mathbf{Y}\|_F^2 \\ &= \arg \min_{\mathbf{X} \in \mathcal{U}_s^{(1:Q)}} \|\mathbf{I}_L - \mathbf{P}\mathbf{X}(\mathbf{X}^\text{H}\mathbf{P}\mathbf{P}\mathbf{X})^\dagger \mathbf{X}^\text{H}\mathbf{P}\|_F^2 \|\mathbf{P}\mathbf{Y}\|_F^2 \\ &= \arg \min_{\mathbf{X} \in \mathcal{U}_s^{(1:Q)}} \|\mathbf{I}_L - (\mathbf{P}\mathbf{X})(\mathbf{P}\mathbf{X})^\dagger\|_F^2 \|\mathbf{P}\mathbf{Y}\|_F^2 \end{aligned}$$

$$= \arg \max_{\mathbf{X} \in U_s^{(1:Q)}} \|\mathbf{P}\mathbf{X}(\mathbf{P}\mathbf{X})^\dagger \mathbf{P}\mathbf{Y}\|_F^2 \quad (47)$$

where, in the last two equalities, we have exploited the fact that  $\mathbf{B}(\mathbf{B}^H \mathbf{B})^\dagger \mathbf{B}^H = \mathbf{B}\mathbf{B}^\dagger$  is the orthogonal projector onto the range of a matrix  $\mathbf{B}$ , and that  $\mathbf{I} - \mathbf{B}\mathbf{B}^\dagger$  is the orthogonal projector onto the null space of  $\mathbf{B}^H$ . When  $\mathbf{X} = \mathbf{x}$  is a column vector, we have

$$\|\mathbf{P}\mathbf{x}(\mathbf{P}\mathbf{x})^\dagger \mathbf{P}\mathbf{Y}\|_F^2 = \|\mathbf{P}\mathbf{x}(\mathbf{x}^H \mathbf{P}\mathbf{x})^{-1} \mathbf{x}^H \mathbf{P}\mathbf{Y}\|_F^2 = \frac{\|\mathbf{P}\mathbf{x}\|^2 \|\mathbf{x}^H \mathbf{P}\mathbf{Y}\|^2}{\|\mathbf{P}\mathbf{x}\|^4} = \frac{\|\mathbf{x}^H \mathbf{P}\mathbf{Y}\|^2}{\|\mathbf{P}\mathbf{x}\|^2} \quad (48)$$

and (47) simplifies to (15).

## REFERENCES

- [1] A. Zhang *et al.*, “Perceptive mobile networks: Cellular networks with radio vision via joint communication and radar sensing,” *IEEE Vehicular Technology Magazine*, vol. 16, no. 2, pp. 20–30, Jun. 2021.
- [2] L. Leyva, D. Castanheira, A. Silva, A. Gameiro, and L. Hanzo, “Cooperative multiterminal radar and communication: A new paradigm for 6G mobile networks,” *IEEE Vehicular Technology Magazine*, vol. 16, no. 4, pp. 38–47, Dec. 2021.
- [3] D. C. Nguyen *et al.*, “6G internet of things: A comprehensive survey,” *IEEE Internet of Things Journal*, vol. 9, no. 1, pp. 359–383, Jan. 2022.
- [4] L. Zheng, M. Lops, Y. C. Eldar, and X. Wang, “Radar and communication coexistence: An overview: A review of recent methods,” *IEEE Signal Processing Magazine*, vol. 36, no. 5, pp. 85–99, Sep. 2019.
- [5] A. Hassanien, M. G. Amin, Y. D. Zhang, and F. Ahmad, “Signaling strategies for dual-function radar communications: an overview,” *IEEE Aerospace and Electronic Systems Magazine*, vol. 31, no. 10, pp. 36–45, Oct. 2016.
- [6] F. Liu, C. Masouros, A. Petropulu, H. Griffiths, and L. Hanzo, “Joint radar and communication design: Applications, state-of-the-art, and the road ahead,” *IEEE Transactions on Communications*, vol. 68, no. 6, pp. 3834 – 3862, Jun. 2020.
- [7] H. Kuschel, D. Cristallini, and K. E. Olsen, “Tutorial: Passive radar tutorial,” *IEEE Aerospace and Electronic Systems Magazine*, vol. 34, no. 2, pp. 2–19, Feb. 2019.
- [8] P. Kumari, J. Choi, N. González-Prelcic, and R. W. Heath, “IEEE 802.11ad-based radar: An approach to joint vehicular communication-radar system,” *IEEE Transactions on Vehicular Technology*, vol. 67, no. 4, pp. 3012–3027, Apr. 2017.
- [9] E. Grossi, M. Lops, L. Venturino, and A. Zappone, “Opportunistic radar in IEEE 802.11ad networks,” *IEEE Transactions on Signal Processing*, vol. 66, no. 9, pp. 2441–2454, May 2018.
- [10] E. Grossi, M. Lops, and L. Venturino, “Adaptive detection and localization exploiting the IEEE 802.11ad standard,” *IEEE Transactions on Wireless Communications*, vol. 19, no. 7, pp. 4394–4407, Jul. 2020.
- [11] E. Grossi, M. Lops, A. M. Tulino, and L. Venturino, “Opportunistic sensing using mmwave communication signals: a subspace approach,” *IEEE Transactions on Wireless Communications*, vol. 20, no. 7, pp. 4420–4434, Jul. 2021.
- [12] J. Choi *et al.*, “Millimeter-wave vehicular communication to support massive automotive sensing,” *IEEE Communications Magazine*, vol. 54, no. 12, pp. 160–167, Dec. 2016.
- [13] H. Stockman, “Communication by means of reflected power,” *Proceedings of the IRE*, vol. 36, no. 10, pp. 1196–1204, Oct. 1948.
- [14] D. Hounam and K.-H. Wagel, “A technique for the identification and localization of SAR targets using encoding transponders,” *IEEE Transactions on Geoscience and Remote Sensing*, vol. 39, no. 1, pp. 3–7, Jan. 2001.
- [15] S. D. Blunt, P. Yatham, and J. Stiles, “Intrapulse radar-embedded communications,” *IEEE Transactions on Aerospace and Electronic Systems*, vol. 46, no. 3, pp. 1185–1200, Jul. 2010.

- [16] S. D. Blunt, J. G. Metcalf, C. R. Biggs, and E. Perrins, "Performance characteristics and metrics for intra-pulse radar-embedded communication," *IEEE Journal on Selected Areas in Communications*, vol. 29, no. 10, pp. 2057–2066, Dec. 2011.
- [17] J. G. Metcalf, C. Sahin, S. D. Blunt, and M. Rangaswamy, "Analysis of symbol-design strategies for intrapulse radar-embedded communications," *IEEE Transactions on Aerospace and Electronic Systems*, vol. 51, no. 4, pp. 2914–2931, Oct. 2015.
- [18] V. Liu *et al.*, "Ambient backscatter: Wireless communication out of thin air," in *Proc. of ACM SIGCOMM*, Hong Kong, China, Aug. 2013, p. 39–50.
- [19] N. Van Huynh *et al.*, "Ambient backscatter communications: A contemporary survey," *IEEE Communications Surveys & Tutorials*, vol. 20, no. 4, pp. 2889–2922, Fourthquarter 2018.
- [20] R. Long, Y.-C. Liang, H. Guo, G. Yang, and R. Zhang, "Symbiotic radio: A new communication paradigm for passive internet of things," *IEEE Internet of Things Journal*, vol. 7, no. 2, pp. 1350–1363, Feb. 2020.
- [21] I. Cnaan-On, S. J. Thomas, J. L. Krolik, and M. S. Reynolds, "Multichannel backscatter communication and ranging for distributed sensing with an FMCW radar," *IEEE Transactions on Microwave Theory and Techniques*, vol. 63, no. 7, pp. 2375–2383, Jul. 2015.
- [22] F. E. Nathanson, J. P. Reilly, and M. N. Cohen, *Radar Design Principles*, 2nd ed. New York, NY, USA: McGraw-Hill Higher Education, 1991.
- [23] M. I. Skolnik, *Introduction to radar systems*, 3rd ed. New York, NY, USA: McGraw-Hill Higher Education, 2015.
- [24] H. Van Trees, *Detection, Estimation, and Modulation Theory: Radar-sonar signal processing and Gaussian signals in noise*. Wiley, 1968.
- [25] G. Wang, F. Gao, R. Fan, and C. Tellambura, "Ambient backscatter communication systems: Detection and performance analysis," *IEEE Transactions on Communications*, vol. 64, no. 11, pp. 4836–4846, Nov. 2016.
- [26] X. Xu, Y.-C. Liang, G. Yang, and L. Zhao, "Reconfigurable intelligent surface empowered symbiotic radio over broadcasting signals," *IEEE Transactions on Communications*, vol. 69, no. 10, pp. 7003–7016, Oct. 2021.
- [27] S. Lin, F. Chen, M. Wen, Y. Feng, and M. Di Renzo, "Reconfigurable intelligent surface-aided quadrature reflection modulation for simultaneous passive beamforming and information transfer," *IEEE Transactions on Wireless Communications*, vol. 21, no. 3, pp. 1469–1481, Mar. 2022.
- [28] J. Proakis and M. Salehi, *Digital Communications*, 5th ed. New York, NY, USA: McGraw-Hill Higher Education, 2014.
- [29] J. A. Tropp and A. C. Gilbert, "Signal recovery from random measurements via orthogonal matching pursuit," *IEEE Transactions on Information Theory*, vol. 53, no. 12, pp. 4655–4666, Dec. 2007.
- [30] J. Liu and X. Wang, "Unsourced multiple access based on sparse tanner graph—efficient decoding, analysis, and optimization," *IEEE Journal on Selected Areas in Communications*, vol. 40, no. 5, pp. 1509–1521, 2022.
- [31] P. Stoica and Y. Selen, "Model-order selection: a review of information criterion rules," *IEEE Signal Processing Magazine*, vol. 21, no. 4, pp. 36–47, Jul. 2004.
- [32] D. Shnidman, "Generalized radar clutter model," *IEEE Transactions on Aerospace and Electronic Systems*, vol. 35, no. 3, pp. 857–865, Jul. 1999.